Clinical and Experimental Pharmacology and Physiology (2005) 32, 952–959

EXOGENOUS NITRIC OXIDE CENTRALLY ENHANCES PULMONARY REACTIVITY IN THE NORMAL AND HYPERTENSIVE RAT

Daryl O Schwenke,* James T Pearson,* Hirotsugu Tsuchimochi,* Hidezo Mori* and Mikiyasu Shirai†

*Department of Cardiac Physiology, National Cardiovascular Center Research Institute, Suita, Osaka and †Faculty of Health Sciences, Hiroshima International University, Hiroshima, Japan

SUMMARY

1. Chronic hypoxia causes sustained pulmonary hypertension and, although impairment of the pulmonary endothelial nitric oxide (NO) pathway has been implicated, no study has described the central role of NO in modulating pulmonary vascular tone and reactivity. Centrally, NO inhibits sympathetic outflow, so we hypothesised that central NO would modulate pulmonary vascular tone and its reactivity to acute hypoxia, especially in the hypertensive state.

2. Male adult Sprague-Dawley rats were exposed to normoxia (N) or chronic hypoxia (CH; 12% O_2) for 14 days. Mean pulmonary arterial pressure (MPAP), systemic mean arterial blood pressure (MABP), cardiac output and heart rate were then measured in pentobarbitone-anaesthetized, artificially ventilated rats. The N and CH rats were exposed to acute hypoxia (10% O_2 for 4 min) after the intracerebroventricular (i.c.v.) administration of artificial cerebrospinal fluid (control) and then again after either i.c.v. N^G-nitro-L-arginine methyl ester (L-NAME; 150 μg in 10 μL) or 3-morpholino-sydnonimine hydrochloride (SIN-1; 100 μg in 10 μL).

3. Chronic hypoxia caused pulmonary hypertension (MPAP 20 ± 1 *vs* 30 ± 1 mmHg in N and CH rats, respectively) and attenuated acute hypoxic pulmonary vasoconstriction (HPV). Central inhibition of NO synthesis (by L-NAME) did not alter baseline MPAP or the acute HPV in either N or CH rats, but it did elevate MABP. The NO donor SIN-1 did not alter baseline MPAP, but it did enhance (N rats) or restore (CH rats) the HPV and decreased MABP.

4. The results of the present study indicate that central NO has a limited role in the tonic modulation of MPAP during normoxia and after chronic hypoxia. However, the acute HPV seems to be enhanced by exogenous NO.

Key words: chronic hypoxia, nitric oxide, pulmonary vasoconstriction, sympathetic nervous system.

INTRODUCTION

Acute alveolar hypoxia causes pulmonary vasoconstriction that is reversible upon re-oxygenation. However, during chronic hypoxia, as is the case with several chronic pulmonary pathological conditions, elevated shear stress within the pulmonary vasculature causes endothelial cell injury/dysfunction,[1] smooth muscle cell proliferation[2] and, inevitably, the irreversible remodelling of the pulmonary vasculature.[3,4] The consequential sustained increase in pulmonary arterial pressure (PAP) increases the workload of the heart and is therefore closely associated with heart failure and increased mortality.

Although the exact cellular mechanisms responsible for the pathogenesis of chronic hypoxia-induced pulmonary arterial hypertension are unknown, alterations in the endothelial nitric oxide (NO) pathway have been implicated as a significant contributing factor.[5,6] Nitric oxide is a potent vasodilator and an inhibitor of vascular remodelling.[7–9] Nitric oxide is produced from L-arginine in a reaction catalysed by isoenzymes of NO synthase (NOS). The synthesis of NO is blocked by several L-arginine analogues, including N^G-nitro-L-arginine methyl ester (L-NAME), which competitively and stereoselectively inhibit the generation of NO from L-arginine.[10]

A reduction in the production of NO has been implicated in the pathophysiology of pulmonary hypertension.[6,8] Endothelial NOS (eNOS)-knockout mice have an increased risk of pulmonary hypertension,[11–13] whereas the hypoxia-induced pulmonary hypertension is attenuated in transgenic mice that overexpress eNOS.[14] In addition, chronic hypoxia limits endogenous NO synthesis,[15] despite an increase in NOS expression.[16–18]

Nitric oxide is produced not only peripherally, but also centrally within various parts of the brain, including the nucleus tractus solitarius (NTS) of the medulla oblongata and the ventrolateral medulla, the cardiovascular regulatory centres.[19–21] Therefore, NO is considered to be involved in the neural regulation of blood pressure, independent of its direct effects on the endothelium of blood vessels.[22] A review by Patel *et al.*[23] reported that the general consensus in the literature was that NO acts as a sympatho-inhibitory substance within the central nervous system. Therefore, central NO inhibition increases sympathetic outflow and, subsequently, arterial blood pressure.[24,25]

The central role of NO in modulating pulmonary vasculature, especially in pathological conditions (e.g. pulmonary hypertension), is still incompletely understood. Yet, as evidence accumulates in support of central NO as an important regulator

Correspondence: Daryl O Schwenke, Department of Cardiac Physiology, National Cardiovascular Center Research Institute, 5-7-1 Fujishirodai, Suita, Osaka 565-8565, Japan. Email: schwenke@ri.ncvc.go.jp

Received 2 March 2005; revision 1 June 2005; accepted 17 July 2005.

of cardiovascular function, the central role of NO in the modulation of the pulmonary vasculature needs to be addressed. Therefore, our first aim in the present study was to elucidate the role of NO in the central modulation of pulmonary vascular tone under normoxic conditions and after the development of chronic hypoxia-induced pulmonary hypertension. Nitric oxide is thought to have an important role in modulating the hypoxic pulmonary vasoconstriction (HPV) in response to acute hypoxic challenges.[26] However, there are conflicting reports as to whether the HPV response is accentuated or attenuated by pulmonary hypertension.[6,27] Therefore, a second aim of the present study was to assess the acute HPV before and after chronic hypoxia and to determine whether central NO has a role in modulating this response.

METHODS

Animals

Experiments were conducted on 23 male Sprague-Dawley rats (8 weeks old; bodyweight approximately 200–280 g). Rats were divided into four groups, as follows: (i) group 1, normoxia (N) + L-NAME; (ii) group 2, chronic hypoxia (CH) + L-NAME; (iii) group 3, N + 3-morpholino-sydnonimine hydrochloride (SIN-1); and (iv) group 4, CH + SIN-1. The CH rats were housed in a hypoxic chamber (12.0 ± 0.1% O_2) continuously for 2 weeks, except for a 10 min interval each day when the chamber was cleaned. The N rats were housed in similar housing, except that N rats breathed room air. The hypoxic gas mixture was delivered to the hypoxic chamber (30 L capacity) at a flow rate of approximately 8 L/min. All rats were on a 12 h light/dark cycle at 25 ± 1°C and were provided with food and water *ad libitum*. All experiments were approved by the local Animal Ethics Committee and conducted in accordance with the guidelines of the Physiological Society of Japan (http://www.soc.nii.ac.jp/psj/).

Anaesthesia and surgery

Rats were initially anaesthetized with pentobarbitone sodium (45 mg/kg, i.p.) and supplementary doses of anaesthetic were administered periodically throughout the experimental protocol (15–30 mg/kg per h, i.p.) so as to maintain a constant surgical level of anaesthesia (assessed by using the limb withdrawal reflex test). Rectal temperature was maintained at 38°C using a rectal thermistor coupled to a thermostatically controlled heating pad.

Using a stereotaxic frame, the tip of a 27 gauge stainless steel cannula was positioned in the right lateral cerebral ventricle based on the coordinates of Paxinos and Watson[28] (0.8 mm posterior to the bregma, 1.5 mm lateral to the midline and 5.0 mm ventral to the skull surface). The distal end of the cannula was connected to a 0.5 mL syringe for subsequent drug administration. Correct positioning of the intracerebroventricular (i.c.v.) catheter was confirmed after each experiment by staining with Evans blue dye (10 μL).

The trachea was cannulated and the lungs ventilated with a rodent ventilator (SN-480-7; Shinano, Tokyo, Japan). The inspirate gas was enriched with O_2 (approximately 50% O_2) and the ventilator settings were adjusted (tidal volume (V_T) approximately 3.5 mL; frequency approximately 80 /min) to maintain arterial P_{CO_2} normocapnic. The femoral artery and vein were cannulated for the measurement of systemic arterial blood pressure and drug administration, respectively. The arterial line contained heparinized saline (50 U/mL). A right thoracotomy was made between the second and third ribs and the conus of the right ventricle was exposed. A 23 gauge needle was used to pierce the ventricle wall and then the gel-filled sensing catheter of a telemetric transmitter (model TA11PA-C40; Data Sciences, St Paul, MN, USA) was inserted anteriorly into the right ventricle and advanced into the pulmonary artery. The catheter was fixed in position with a 7.0 Prolene suture to the pericardium. The aorta was blunt dissected free from the pulmonary artery and a transonic perivascular flowprobe (model 2RB; Transonic Systems, Ithaca, NY, USA) was positioned around the ascending aorta for the continuous measurement of cardiac output.

Drugs

Artificial cerebrospinal fluid (aCSF) was used as the vehicle for administering the NOS inhibitor L-NAME and the slow-releasing NO donor, 3-[4-morpholinyl]-sydnonimine-hydrochloride (SIN-1). The aCSF (pH 7.36–7.43) was comprised of 150 mmol/L NaCl, 3.0 mmol/L KCl, 0.8 mmol/L $MgCl_2$, 1.4 mmol/L $CaCl_2$ and 1.0 mmol/L Na phosphate. Intracerebroventricular injections were given as a 10 μL bolus over 30 s. Intravenous (i.v.) injections were administered as a 0.2 mL bolus over 15 s, followed by a 0.1 mL saline flush.

Measurement of right ventricular weight

Immediately following the experiment, rats were killed by anaesthetic overdose, the heart was excised, the atria were removed and the right ventricle wall was separated from the left ventricle, including the septum. Tissues were blotted and weighed. Right and left ventricular weights were expressed as the ratio of the right ventricle to the left ventricular + septum weight ($W_{RV}/W_{LV+septum}$; Fulton's ratio).

Experimental protocols

Once all variables had stabilized after surgery (approximately 20 min), baseline values were recorded for 10 min in response to the i.c.v. administration of aCSF (10 μL). The inspirate was then switched to hypoxia (10% O_2 balanced by N_2) for 4 min. Upon recovery from acute hypoxia, rats received a bolus i.c.v. injection of either L-NAME (150 μg; groups 1 and 2) or SIN-1 (100 μg; groups 3 and 4). After 5 (L-NAME) or 10 min (SIN-1), the acute hypoxic test was repeated. After a further 10 min, once variables had recovered to prehypoxic values, rats (groups 1 and 2 only) received a bolus i.v. injection of L-NAME (50 mg/kg) and acute hypoxia was tested 10 min later.

Data acquisition and analysis

Pulmonary arterial pressure was measured using telemetry. The signal from the implanted transmitter (model TA11PA-C20; Data Sciences) was calibrated in reference to an input from an ambient-pressure monitor (C11PR; Data Sciences) and subsequently relayed to a personal computer. Cardiac output (CO) was measured continuously from the ascending aorta using a Transonic small animal blood flowmeter (model T206; Transonic Systems) with a flowprobe (model 2RB). Arterial blood pressure (ABP) was measured continuously with a Deltran pressure transducer (Utah Medical Products, Midvale, UT, USA) and the signal was relayed to a Powerlab bridge amplifier (ML117; ADInstruments, Tokyo, Japan).

The signals for ABP, CO and PAP were relayed from their respective units and sampled continuously at 200 Hz with an eight-channel MacLab/8s interface hardware system (ADInstruments) and recorded on a Macintosh Power Book G4 using Chart (v. 5.0.1; ADInstruments). Heart rate (HR) was derived from the arterial systolic peaks. Cardiac output was normalized (off-line) to 100 g bodyweight. Total systemic vascular resistance (SVR) and total pulmonary vascular resistance (PVR) were calculated by dividing mean ABP (MABP) and mean PAP (MPAP) by the normalized CO. A 10 block of data was analysed −60, −30 s and immediately before (time '0') acute hypoxic exposure and then after 20, 40, 60, 90, 120, 180 and 240 s of exposure to 10% O_2. Normoxic data for individual rats in each group were averaged from values acquired at −60, −30 s and at time 0. An arterial blood sample (0.1 mL) was extracted 5 min after the completion of surgery for analysis of arterial P_{CO_2} using an ABL 605 blood gas analyser (Radiometer, Copenhagen, Denmark). An additional 0.1 mL was extracted to measure haematocrit.

Statistical analysis

All statistical analyses were conducted using Statview (v. 5.01; SAS Institute, Cary, NC, USA). All results are presented as the mean±SEM. Two-way ANOVA (repeated measures) was used to test significance for: (i) changes in each variable in response to 4 min of acute hypoxia; and (ii) whether the hypoxic response was altered by drug administration (i.c.v. or i.v.).

One-way ANOVA (factorial) was used to test for differences in baseline values for normoxic and chronic hypoxic groups of rats. Where statistical significance was reached, post hoc analyses were incorporated using the paired or unpaired *t*-test with Dunnet's correction for multiple comparisons. $P \leq 0.05$ was predetermined as the level of significance for all statistical analyses.

RESULTS

Chronic hypoxia induced pulmonary hypertension (Table 1), as evidenced by the observation that the MPAP and PVR of CH rats ($n = 11$) was 50 and 34% higher, respectively, than that of normoxic (N) rats ($n = 12$; $P < 0.01$). Consequently, CH rats developed right ventricular hypertrophy (ΔRV/LV + Sep ratio of 0.23). Chronic hypoxia did not significantly change MABP or CO, but it did cause a significant reduction in HR (ΔHR 37 b.p.m.; $P < 0.01$), suggesting that the development of right ventricular hypertrophy resulted in an increase in stroke volume. An increase in haematocrit (ΔHct 18%; $P < 0.001$) also occurred in CH.

Responses to acute hypoxia

In N rats, acute exposure to 10% O_2 provoked an increase in MPAP, after a latency of 65–88 s, which reached a plateau after approximately 180 s (Fig. 1a). By 4 min, MPAP had increased significantly by 31 ± 5%, in spite of a small, albeit not significant, decline in both HR (6 ± 1%) and CO (16 ± 6%), reflecting substantial pulmonary vasoconstriction (67 ± 13% increase in PVR). Acute hypoxia also provoked a 56 ± 2% decrease in MABP by the end of the 4th min, which was primarily due to systemic vasodilatation (46 ± 3% decrease in SVR; Fig. 1a). Although CH slightly altered baseline values (detailed above), the magnitude of the response to 4 min hypoxia for MABP, HR, CO and SVR was essentially the same for the CH and N groups of rats (Fig. 1a,b). However, the potent pulmonary vasoconstriction seen in N rats was abolished in CH rats. Consequently, exposure to 10% O_2 did not cause a significant increase in MPAP or PVR in CH rats.

Administration of L-NAME

The maximum cardiovascular responses following a single i.c.v injection of L-NAME are given in Table 2. In N rats, L-NAME caused a small (<3% increase) but consistent increase in PVR ($P < 0.05$), although MPAP was not significantly affected. In addition, L-NAME caused a maximal 15 ± 4% increase in MABP after 35 ± 8 s, which was solely attributed to systemic vasoconstriction (16 ± 4% increase in SVR). All other variables were unaltered. The PVR, MABP and SVR responses were brief, returning to pre-L-NAME values within 4.5 min. Consequently, because acute hypoxia was tested 5 min after L-NAME injection, the prehypoxia baseline data were similar before and after L-NAME treatment. Furthermore, the magnitude of the cardiovascular responses to L-NAME for CH rats was statistically similar to that of N rats (Table 2). The i.c.v. administration of L-NAME did

Table 1 Baseline cardiovascular variables in rats exposed to normoxic or chronic hypoxia

	N rats	CH rats
MPAP (mmHg)	20.2 ± 1.1	30.4 ± 1.2**
MABP (mmHg)	106 ± 6	118 ± 4
CO (mL/min/100 g)	11.17 ± 0.75	12.32 ± 0.53
HR (b.p.m.)	416 ± 8	379 ± 11*
SVR (mmHg/mL per min per 100 g)	9.73 ± 0.64	9.72 ± 0.53
PVR (mmHg/mL per min per 100 g)	1.88 ± 0.14	2.52 ± 0.15*
RV/LV + Septum	0.31 ± 0.01	0.55 ± 0.02**
Haematocrit (%)	47 ± 1	65 ± 1**

Data are the mean±SEM. *$P < 0.01$, **$P < 0.001$ compared with normoxia values.

N, normoxic rats (groups 1 and 3; $n = 12$); CH, chronic-hypoxic rats (12% O_2 for 2 weeks; groups 2 and 4; $n = 11$); MPAP, mean pulmonary arterial pressure; MABP, mean arterial blood pressure; CO, cardiac output; HR, heart rate; SVR, systemic vascular resistance; PVR, pulmonary vascular resistance; RV, right ventricle; LV, left ventricle.

Table 2 Maximum responses to intracerebroventricular N^G-nitro-L-arginine methyl ester (150 μg in 10 μL) in normoxic rats ($n = 7$) and chronic hypoxic rats ($n = 5$)

	Normoxia		Chronic hypoxia	
	Pre-L-NAME	Max L-NAME	Pre-L-NAME	Max L-NAME
MPAP (mmHg)	18.6 ± 0.6	19.0 ± 0.6	30.4 ± 1.6	31.1 ± 1.9
MABP (mmHg)	102 ± 10	116 ± 8**	110 ± 5	120 ± 5*
CO (mL/min per 100 g)	10.12 ± 1.10	10.09 ± 1.13	12.24 ± 1.07	11.98 ± 1.00
HR (b.p.m.)	413 ± 10	416 ± 9	373 ± 13	376 ± 14
SVR (mmHg/mL per min per 100 g)	10.79 ± 1.85	12.39 ± 2.05**	9.14 ± 0.55	10.19 ± 0.66*
PVR (mmHg/mL per min per 100 g)	1.94 ± 0.20	2.00 ± 0.21*	2.53 ± 0.18	2.64 ± 0.21*

Data are the mean±SEM. *$P < 0.05$, **$P < 0.01$ compared with pre-N^G-nitro-L-arginine methyl ester (L-NAME).

MPAP, mean pulmonary arterial pressure; MABP, mean arterial blood pressure; CO, cardiac output; HR, heart rate; SVR, systemic vascular resistance; PVR, pulmonary vascular resistance.

not alter the acute hypoxic response for any of the variables recorded in either N or CH rats (Fig. 1a,b).

Cardiovascular responses to the i.v. administration of L-NAME (50 mg/kg, i.v.) were also recorded. In N rats, a bolus i.v. dose of L-NAME provoked robust systemic vasoconstriction (123 ± 20% increase in SVR; $P < 0.001$), as well as, to a lesser extent, pulmonary vasoconstriction (80 ± 10% increase in PVR; $P < 0.01$). The baroreflex decrease in HR and CO (NS; see baseline data in Fig. 1a,b) meant that the changes in vascular resistance were accompanied by smaller, but still significant, increases in MABP (42 ± 18% increase in MABP; $P < 0.001$) and MPAP (13 ± 9% increase in MPAP; NS) in N rats. After 2 weeks of chronic hypoxia, L-NAME (i.v.) had a similar effect on the systemic vasculature and caused a similar depression of HR (NS) and CO ($P < 0.001$), but it had a more pronounced effect on the pulmonary vasculature (24 ± 5% increase in MPAP (NS); 116 ± 18% increase in PVR ($P < 0.01$)).

Treatment of N rats with L-NAME (i.v.) exacerbated the reduction in MABP and SVR in response to acute hypoxia and accentuated the increase in MPAP and PVR (Fig. 1a,b). Despite a depression in baseline values for CO and HR, i.v. administration of L-NAME did not change the transient responses to hypoxia. In CH rats, the transient MABP and SVR responses to acute hypoxia were elevated by L-NAME (i.v.). In addition, L-NAME restored the potent MPAP (and PVR) response to acute hypoxia (observed in N rats), which had been absent prior to L-NAME treatment (Fig. 1a,b).

Administration of SIN-1

Following a single bolus i.c.v. injection of SIN-1 (100 μg) in N rats, baseline MPAP and PVR were not significantly altered. However, MABP declined slowly before stabilizing 38 ± 7% below the pre-SIN-1 baseline (Table 3). Preliminary studies

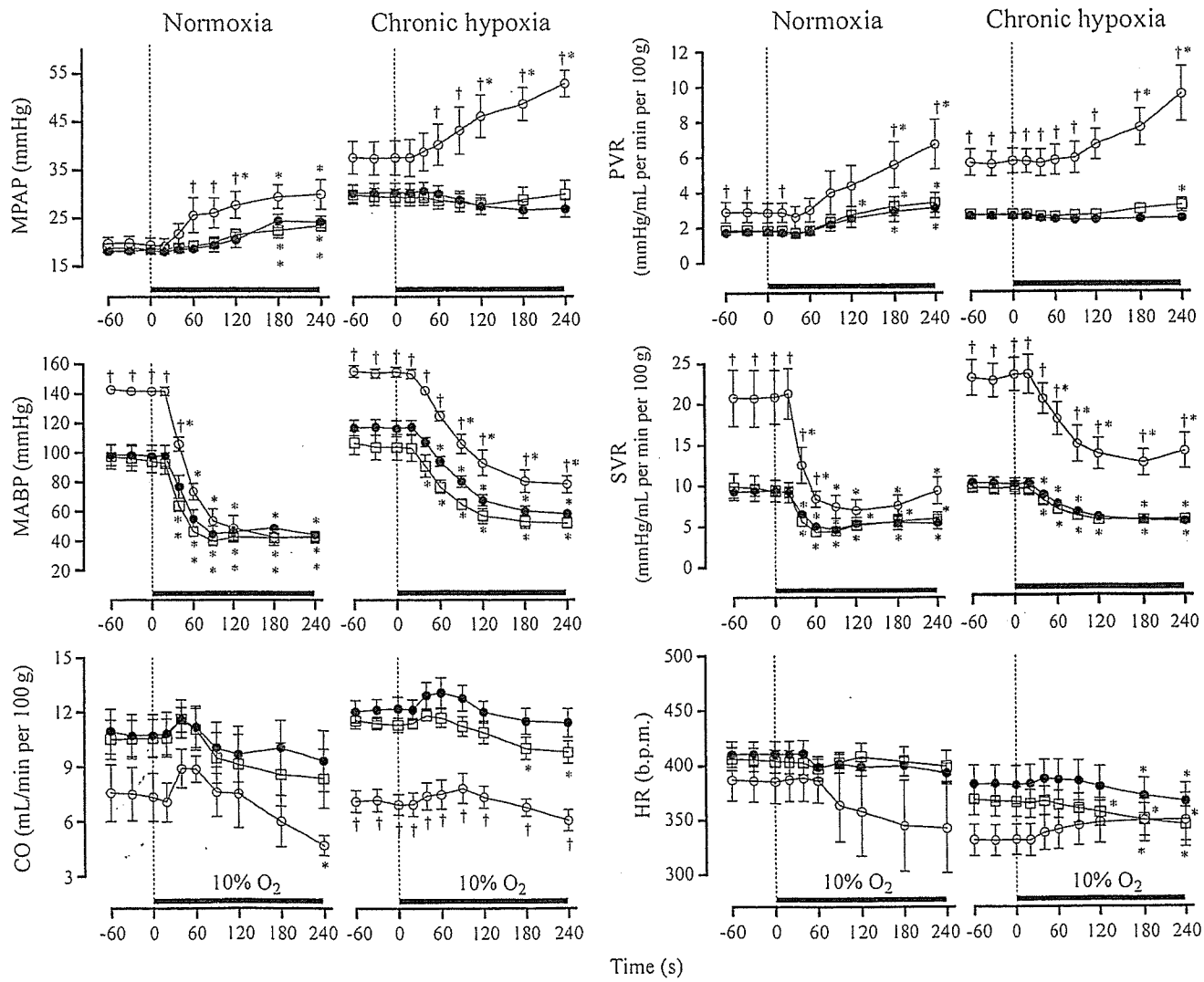

Fig. 1 Mean pulmonary arterial pressure (MPAP), mean arterial blood pressure (MABP), cardiac output (CO), pulmonary vascular resistance (PVR), systemic vascular resistance (SVR) and heart rate (HR) responses to acute hypoxia (10% O_2 for 4 min) in normoxic (N) rats ($n = 7$) and chronic hypoxic (CH) rats ($n = 5$), before (●) and after the administration of N^G-nitro-L-arginine methyl ester (L-NAME; □, 150 μg in 10 μL, i.c.v.; ◇, 50 mg/kg, i.v.). $^*P < 0.05$ compared with pre-acute hypoxia values; $^\dagger P < 0.05$ compared with L-NAME values.

showed that once cardiovascular variables stabilized following the initial response to SIN-1, variables did not change for at least another 20 min. The fall in MABP was primarily attributed to vasodilatation (29 ± 7% decrease in SVR; $P < 0.05$). In CH rats, SIN-1 (i.c.v.) did not alter PVR, but it did decrease MPAP by 21 ± 3% ($P < 0.01$) owing to a 22 ± 5% decrease in CO ($P < 0.05$). Syndnonimine-1 provoked a larger decrease in CO in CH rats (22 ± 5% decrease; $P < 0.05$), so that the fall in MABP was also greater in CH rats (46 ± 3% decrease), because the decline in SVR was similar for N rats and CH rats (27 ± 7 and 29% decrease in SVR, respectively).

In N rats, the CO response to acute hypoxia was depressed by SIN-1 so that, even though the MPAP response appeared to be unchanged (Fig. 2a), the PVR response to hypoxia was accentuated by SIN-1 (64 ± 24 and 127 ± 26% increase, respectively; Fig. 2b). Syndnonimine-1 reduced the magnitude of the MABP and SVR responses to hypoxia, although the absolute MABP (and SVR) values during hypoxia before and after SIN-1 were similar. In addition, SIN-1 abolished the small hypoxia-induced decline in HR observed prior to SIN-1 administration.

In CH rats, SIN-1 restored the pulmonary vasoconstriction in response to acute hypoxia. This was evident by a 33 ± 5% increase in MPAP (cf. a 3% increase for control) and a 90 ± 11% increase in PVR (cf. a 20% increase for control). The effect of SIN-1 on the MABP, SVR, CO and HR responses to acute hypoxia were similar for N and CH rats (Fig. 2a,b).

DISCUSSION

To date, this is the first study to investigate the central role of NO in: (i) modulating MPAP in the normal and hypertensive state; and (ii) acute HPV. The primary findings of the present study show that, in both N and CH rats, the acute central inhibition of NOS does not appear to modulate baseline MPAP or pulmonary vascular

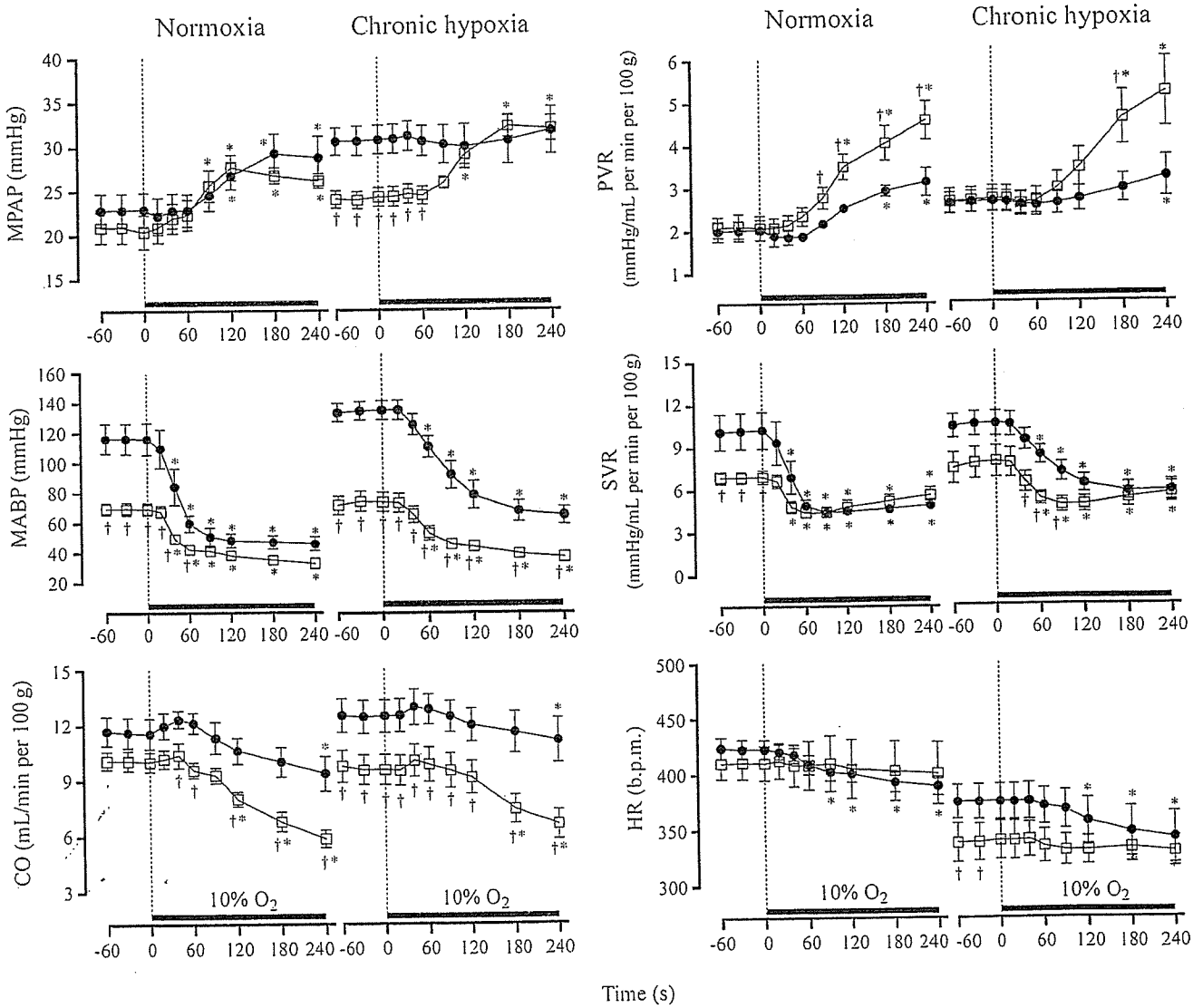

Fig. 2 Effect of i.c.v. syndnonimine-1 (SIN-1) on mean pulmonary arterial pressure (MPAP), mean arterial blood pressure (MABP), cardiac output (CO), pulmonary vascular resistance (PVR), systemic vascular resistance (SVR) and heart rate (HR) responses to acute hypoxia (10% O_2 for 4 min) in normoxic (N) rats ($n = 5$) and chronic hypoxic (CH) rats ($n = 6$). (●), control (artificial cerebrospinal fluid); (□), SIN-1 (100 μg in 10 μL). *$P < 0.05$ compared with pre-acute hypoxia values; †$P < 0.05$ compared with SIN-1-values.

in MPAP because of the potential opposing effects of α- and β-adrenoceptor activation within the pulmonary vasculature.

In the present study, as well as in other studies, the central administration of NO donors has been shown to reduce MABP.[25,43] Nurminen and Vapaatalo[44] also showed that certain NO-releasing substances, such as nitroprusside, reduced MABP, although they also mentioned that the central administration of SIN-1 (approximately 600 μg/kg) increased MABP.

At high doses, SIN-1 can cogenerate NO and superoxide anions.[45,46] Furthermore, an increase in the central generation of superoxide anions has been reported to increase sympathetic activity and, consequently, ABP.[47] Therefore, the increase in MABP in the study of Nurminen and Vapaatalo[44] may be attributed to the formation of superoxide anions. At low doses, the superoxide-associated effects of SIN-1 are significantly outweighed by the actions of NO.[45] Therefore, because the present study used a comparatively low dose of SIN-1 (100 μg), we interpret the decrease in MABP to indicate that, at this dose, SIN-1 was acting solely as an NO donor.

The decrease in MABP following the central administration of exogenous NO has been attributed to a decrease in sympathetic activity.[40,48] To date, the present study is the first to investigate the effects of a central NO donor on MPAP. The important finding of the present study is that exogenous NO did not directly alter baseline pulmonary vascular tone (i.e. PVR was not altered), but it did enhance (in N rats) or restore (in CH rats) the acute HPV response. These results support the idea that central NO has little influence on the tonic modulation of pulmonary vascular tone, although it enhances the acute HPV.

Although we cannot confirm the underlying mechanisms responsible for these observations, it is possible that SIN-1 did reduce sympathetic activity in the rats in the present study, subsequently enhancing the HPV. Shirai *et al.*[49] demonstrated that β-adrenoceptor blockade had only a minor effect on baseline pulmonary vascular tone in normoxia, but it significantly accentuated the acute HPV (α-adrenoceptor blockade had no effect on the magnitude of the HPV). This observation may explain the reason as to why central SIN-1 did not affect baseline PVR but accentuated the HPV in the present study. Although PVR was not affected, central SIN-1 did reduce MPAP in the present study (significantly in CH rats), solely due to a reduction in CO. This, too, may be due to a reduction in β-adrenoceptor activity, because β-adrenoceptor attenuation has been reported to significantly reduce CO.[50,51]

The mechanism(s) responsible for the attenuation of the HPV after chronic hypoxia remain poorly understood. However, it is possible to speculate that β-adrenoceptor upregulation may be one contributing factor because previous studies have shown that chronic hypoxia significantly increases β-adrenoceptor numbers within the lung.[52,53] Changes in β-adrenoceptor availability during chronic hypoxia could potentially limit the development of pulmonary hypertension and, therefore, be physiologically beneficial; an important area that warrants further research.

In summary, we have shown that central NO has a limited role in modulating tonic MPAP in the normal and hypertensive states. However, exogenous NO enhanced the acute HPV, although central NO inhibition had no effect on the acute HPV. Whether central NO acts to inhibit β-adrenoceptor-mediated vasodilation of the acute HPV is another area that warrants further investigation. The present study used an anaesthetized preparation to investigate the modulation of MPAP in normoxia and after chronic hypoxia. We did not, however, address any potential changes in the control of MPAP during the development of pulmonary hypertension. Hampl and Herget[38] indicated that, during the development of pulmonary hypertension, NO was essential in preventing pulmonary hypertension in the early stages, but became insignificant in the latter stages owing to endothelial dysfunction. Therefore, we will subsequently develop a conscious, chronically cannulated rat model to monitor the development of pulmonary hypertension during the chronic central inhibition/infusion of NO.

ACKNOWLEDGEMENT

The authors are very grateful for the aid and support provided by the Japan Society for the Promotion of Science (JSPS).

REFERENCES

1. Archer S, Rich S. Primary pulmonary hypertension: A vascular biology and translational research 'work in progress'. *Circulation* 2000; **102**: 2781–91.
2. Mandegar M, Yuan JX. Role of K^+ channels in pulmonary hypertension. *Vasc. Pharmacol.* 2002; **38**: 25–33.
3. Barbera JA, Peinado VI, Santos S. Pulmonary hypertension in COPD: Old and new concepts. *Monaldi Arch. Chest Dis.* 2000; **55**: 445–9.
4. Voelkel NF, Tuder RM. Hypoxia-induced pulmonary vascular remodeling: A model for what human disease? *J. Clin. Invest.* 2000; **106**: 733–8.
5. Fike CD, Kaplowitz MR, Thomas CJ, Nelin LD. Chronic hypoxia decreases nitric oxide production and endothelial nitric oxide synthase in newborn pig lungs. *Am. J. Physiol.* 1998; **274**: L517–26.
6. Huang KL, Wu CP, Kang BH, Lin YC. Chronic hypoxia attenuates nitric oxide-dependent hemodynamic responses to acute hypoxia. *J. Biomed. Sci.* 2002; **9**: 206–12.
7. Cornwell TL, Arnold E, Boerth NJ, Lincoln TM. Inhibition of smooth muscle cell growth by nitric oxide and activation of cAMP-dependent protein kinase by cGMP. *Am. J. Physiol.* 1994; **267**: C1405–13.
8. Le Cras TD, McMurtry IF. Nitric oxide production in the hypoxic lung. *Am. J. Physiol. Lung Cell. Mol. Physiol.* 2001; **280**: L575–82.
9. Sato J, Nair K, Hiddinga J *et al.* eNOS gene transfer to vascular smooth muscle cells inhibits cell proliferation via upregulation of p27 and p21 and not apoptosis. *Cardiovasc. Res.* 2000; **47**: 697–706.
10. Palmer RM, Rees DD, Ashton DS, Moncada S. L-Arginine is the physiological precursor for the formation of nitric oxide in endothelium-dependent relaxation. *Biochem. Biophys. Res. Commun.* 1988; **153**: 1251–6.
11. Fagan KA, Fouty BW, Tyler RC *et al.* The pulmonary circulation of homozygous or heterozygous eNOS-null mice is hyperresponsive to mild hypoxia. *J. Clin. Invest.* 1999; **103**: 291–9.
12. Steudel W, Ichinose F, Huang PL *et al.* Pulmonary vasoconstriction and hypertension in mice with targeted disruption of the endothelial nitric oxide synthase (NOS 3) gene. *Circ. Res.* 1997; **81**: 34–41.
13. Steudel W, Scherrer-Crosbie M, Bloch KD *et al.* Sustained pulmonary hypertension and right ventricular hypertrophy after chronic hypoxia in mice with congenital deficiency of nitric oxide synthase 3. *J. Clin. Invest.* 1998; **101**: 2468–77.
14. Ozaki M, Kawashima S, Yamashita T *et al.* Reduced hypoxic pulmonary vascular remodeling by nitric oxide from the endothelium. *Hypertension* 2001; **37**: 322–7.
15. Sato K, Rodman DM, McMurtry IF. Hypoxia inhibits increased ET_B receptor-mediated NO synthesis in hypertensive rat lungs. *Am. J. Physiol.* 1999; **276**: L571–81.
16. Xue C, Rengasamy A, Le Cras TD, Koberna PA, Dailey GC, Johns RA. Distribution of NOS in normoxic vs. Hypoxic rat lung:

Upregulation of NOS by chronic hypoxia. *Am. J. Physiol.* 1994; **267**: L667–78.
17. Shirai M, Pearson JT, Shimouchi A *et al.* Changes in functional and histological distributions of nitric oxide synthase caused by chronic hypoxia in rat small pulmonary arteries. *Br. J. Pharmacol.* 2003; **139**: 899–910.
18. Le Cras TD, Xue C, Rengasamy A, Johns RA. Chronic hypoxia upregulates endothelial and inducible NO synthase gene and protein expression in rat lung. *Am. J. Physiol.* 1996; **270**: L164–70.
19. Matsumura K, Tsuchihashi T, Kagiyama S, Abe I, Fujishima M. Role of nitric oxide in the nucleus of the solitary tract of rats. *Brain Res.* 1998; **798**: 232–8.
20. Zanzinger J, Czachurski J, Seller H. Inhibition of basal and reflex-mediated sympathetic activity in the RVLM by nitric oxide. *Am. J. Physiol.* 1995; **268**: R958–62.
21. Ohta A, Takagi H, Matsui T, Hamai Y, Iida S, Esumi H. Localization of nitric oxide synthase-immunoreactive neurons in the solitary nucleus and ventrolateral medulla oblongata of the rat: Their relation to catecholaminergic neurons. *Neurosci. Lett.* 1993; **158**: 33–5.
22. Garthwaite J, Boulton CL. Nitric oxide signaling in the central nervous system. *Annu. Rev. Physiol.* 1995; **57**: 683–706.
23. Patel KP, Li YF, Hirooka Y. Role of nitric oxide in central sympathetic outflow. *Exp. Biol. Med.* 2001; **226**: 814–24.
24. Hironaga K, Hirooka Y, Matsuo I *et al.* Role of endogenous nitric oxide in the brain stem on the rapid adaptation of baroreflex. *Hypertension* 1998; **31**: 27–31.
25. Nishimura M, Takahashi H, Nanbu A, Sakamoto M, Yoshimura M. Cardiovascular regulation by L-arginine in the brain of rats: Role of the brain renin–angiotensin system and nitric oxide. *Am. J. Hypertens.* 1997; **10**: 389–96.
26. Clini E, Ambrosino N. Nitric oxide and pulmonary circulation. *Med. Sci. Monit.* 2002; **8**: RA178–82.
27. Weissmann N, Nollen M, Gerigk B *et al.* Downregulation of hypoxic vasoconstriction by chronic hypoxia in rabbits: Effects of nitric oxide. *Am. J. Physiol. Heart Circ. Physiol.* 2003; **284**: H931–8.
28. Paxinos G, Watson C. *The Brain in Stereotaxic Coordinates*, 4th edn. Academic Press, San Diego, CA. 1998.
29. Ao Q, Huang L, Zhu P, Xiong M, Wang D. Inhibition of expression of hypoxia-inducible factor-1alpha mRNA by nitric oxide in hypoxic pulmonary hypertension rats. *J. Huazhong Univ. Sci. Technol. Med. Sci.* 2004; **24**: 5–8.
30. Hampl V, Archer SL, Nelson DP, Weir EK. Chronic EDRF inhibition and hypoxia: Effects on pulmonary circulation and systemic blood pressure. *J. Appl. Physiol.* 1993; **75**: 1748–57.
31. Coney AM, Bishay M, Marshall JM. Influence of endogenous nitric oxide on sympathetic vasoconstriction in normoxia, acute and chronic systemic hypoxia in the rat. *J. Physiol.* 2004; **555**: 793–804.
32. Adnot S, Raffestin B, Eddahibi S, Braquet P, Chabrie PE. Loss of endothelium-dependent relaxant activity in the pulmonary circulation of rats exposed to chronic hypoxia. *J. Clin. Invest.* 1991; **87**: 155–62.
33. Bansinath M, Arbabha B, Turndorf H, Garg UC. Chronic administration of a nitric oxide synthase inhibitor *N*-nitro-L-arginine, and drug-induced increase in cerebellar cyclic GMP *in vivo*. *Neurochem. Res.* 1993; **18**: 1063–6.
34. Nurminen ML, Ylikorkala A, Vapaatalo H. Central inhibition of nitric oxide synthesis increases blood pressure and heart rate in anesthetized rats. *Methods Fundam. Exp. Clin. Pharmacol.* 1997; **19**: 35–41.
35. Fletcher EC. Invited review: Physiological consequences of intermittent hypoxia: Systemic blood pressure. *J. Appl. Physiol.* 2001; **90**: 1600–5.
36. Harada S, Tokunaga S, Momohara M *et al.* Inhibition of nitric oxide formation in the nucleus tractus solitarius increases renal sympathetic nerve activity in rabbits. *Circ. Res.* 1993; **72**: 511–16.
37. Zanzinger J, Czachurski J, Seller H. Nitric oxide in the ventrolateral medulla regulates sympathetic responses to systemic hypoxia in pigs. *Am. J. Physiol.* 1998; **275**: R33–9.
38. Hampl V, Herget J. Role of nitric oxide in the pathogenesis of chronic pulmonary hypertension. *Physiol. Rev.* 2000; **80**: 1337–72.
39. Choi KC, Jung M, Lee JU, Kim SW, Kim NH, Kang YJ. Attenuated central pressor response to nitric oxide synthesis inhibition in chronic renal failure rats. *Korean J. Intern. Med.* 1997; **12**: 58–61.
40. Togashi H, Sakuma I, Yoshioka M *et al.* A central nervous system action of nitric oxide in blood pressure regulation. *J. Pharmacol. Exp. Ther.* 1992; **262**: 343–7.
41. Shirai M, Shindo T, Shimouchi A, Ninomiya I. Diameter and flow velocity changes of feline small pulmonary vessels in response to sympathetic nerve stimulation. *Pflügers Arch.* 1994; **429**: 267–73.
42. Shirai M, Matsukawa K, Nishiura N, Kawaguchi AT, Ninomiya I. Changes in efferent pulmonary sympathetic nerve activity during systemic hypoxia in anesthetized cats. *Am. J. Physiol.* 1995; **269**: R1404–9.
43. Matsumura K, Abe I, Tsuchihashi T, Fujishima M. Central nitric oxide attenuates the baroreceptor reflex in conscious rabbits. *Am. J. Physiol.* 1998; **274**: R1142–9.
44. Nurminen ML, Vapaatalo H. Effect of intracerebroventricular and intravenous administration of nitric oxide donors on blood pressure and heart rate in anaesthetized rats. *Br. J. Pharmacol.* 1996; **119**: 1422–6.
45. Stopper H, Moller M, Bommel HM, Schmidt HH. Cytotoxic versus genotoxic effects of nitric oxide (NO). *Toxicol. Lett.* 1999; **106**: 59–67.
46. Megson IL, Webb DJ. Nitric oxide donor drugs: Current status and future trends. *Expert Opin. Investig. Drugs* 2002; **11**: 587–601.
47. Gao L, Wang W, Li YL *et al.* Superoxide mediates sympathoexcitation in heart failure: Roles of angiotensin II and NAD(P)H oxidase. *Circ. Res.* 2004; **95**: 937–44.
48. Shapoval LN, Sagach VF, Pobegailo LS. Nitric oxide influences ventrolateral medullary mechanisms of vasomotor control in the cat. *Neurosci. Lett.* 1991; **132**: 47–50.
49. Shirai M, Shindo T, Ninomiya I. β-Adrenergic mechanisms attenuated hypoxic pulmonary vasoconstriction during systemic hypoxia in cats. *Am. J. Physiol.* 1994; **266**: H1777–85.
50. Kontos HA, Lower RR. Role of beta-adrenergic receptors in the circulatory response to hypoxia. *Am. J. Physiol.* 1969; **217**: 756–63.
51. Chiong MA, Hatcher JD. The sympathoadrenergic system in the cardiovascular responsess to hypoxia in the dog. *Can. J. Physiol. Pharmacol.* 1972; **50**: 674–83.
52. Birnkrant DJ, Davis PB, Ernsberger P. Visualization of high- and low-affinity beta-adrenergic receptors in rat lung: Upregulation by chronic hypoxia. *Am. J. Physiol.* 1993; **265**: L389–94.
53. Winter RJ, Dickinson KE, Rudd RM, Sever PS. Tissue specific modulation of beta-adrenoceptor number in rats with chronic hypoxia with an attenuated response to down-regulation by salbutamol. *Clin. Sci.* 1986; **70**: 159–65.

Enhanced Functional Gap Junction Neoformation by Protein Kinase A–Dependent and Epac-Dependent Signals Downstream of cAMP in Cardiac Myocytes

Satoshi Somekawa, Shigetomo Fukuhara, Yoshikazu Nakaoka, Hisakazu Fujita, Yoshihiko Saito, Naoki Mochizuki

Abstract—Gap junctions (GJs) constituted by neighboring cardiac myocytes are essential for gating ions and small molecules to coordinate cardiac contractions. cAMP is suggested to be a potent stimulus for enhancement of GJ function. However, it remains elusive how cAMP potentiates the GJ of cardiomyocytes. Here we demonstrated that the gating function of GJ is enhanced by the protein kinase A (PKA)–dependent signal, and that the accumulation of connexin43 (Cx43), the most abundant Cx in myocytes, is enhanced by an exchange protein directly activated by cAMP (Epac) (Rap1 activator)–dependent signal. The gating function of GJs was analyzed by microinjected dye transfer method. The accumulation of Cx43 was analyzed by quantitative immunostaining. Using the PKA-specific activator N^6-benzoyladenosine-3′,5′-cyclic monophosphate (6Bnz) and Epac-specific activator 8-(4-chlorophenylthio)-2′-*O*-methyladenosine-3′,5′-cyclic monophosphate (8CPT), we could delineate the two important downstream signals of cAMP for enhanced GJ neoformation. Whereas 6Bnz potentiated gating function of GJs with slight accumulation of Cx43 at cell–cell contacts, 8CPT remarkably enhanced the accumulation of Cx43 with a slight effect on gating. We further noticed that adherens junctions (AJs) were maturated by 8CPT, as marked by increased neural-cadherin immunostaining. Because AJ formation precedes the GJ formation, AJ formation accelerated by Epac-Rap1 signal may result in enhanced GJ formation. The involvement of Epac-Rap1 signal in GJ neoformation was further confirmed by evidence that inactivation of Rap1 by overexpression of Rap1GAP1b perturbed the accumulation of Cx43 at cell–cell contacts. Collectively, PKA and Epac cooperatively enhance functional GJ neoformation in cardiomyocytes. (***Circ Res.* 2005;97:655-662.**)

Key Words: gap junction ■ connexin43 ■ myocardial structure ■ cardiac gap junction connexins

Gap junctions (GJs) are channels formed by two docking connexons; one connexon is provided by each of the two contiguous cells and is constituted of six connexin (Cx) molecules.[1] Among the 20 Cx members, Cx40, Cx43, and Cx45 are expressed in the heart.[2] Of the three, Cx43 is predominantly expressed in working heart muscle cells.[3,4] GJs in the heart are characterized by their localization at the intercalated disk between each myocyte and also by their role in electrical conductance required for coordinated electrical excitation.[5] Myocytes electrically coupled by GJs show synchronized contraction. The importance of Cx43 in electrical excitation in vivo is evident by cardiac-specific depletion of Cx43 leading to cardiac arrhythmia.[6]

The overall function of GJs depends on the number of GJs and the gating function of assembled GJs. GJs are upregulated by increased transcription of Cx, increased distribution of Cx at cell–cell contacts, and decreased degradation of Cx from the cell membrane. cAMP increases Cx43 mRNA.[7] cAMP also enhances the trafficking of Cx43 from the endoplasmic reticulum/Golgi apparatus to the plasma membrane.[8] Cx43 turnover is regulated by proteosomal and lysosomal degradation, and the half-life of Cx43 is less than two hours, suggesting that a rapid synthesis and trafficking system operates in cardiac myocytes.[9]

GJ is modulated by the phosphorylation of Cx43 on Ser and Tyr residues. The intercellular communication through Cx43 is decelerated and accelerated by its phosphorylation on Ser368 by protein kinase C and on Ser364 by protein kinase A (PKA), respectively.[10,11] In addition to Ser phosphorylation, phosphorylated Cx43 on Tyr247 and Tyr265 is repressed from junctional communication.[12] In addition to phosphorylation, GJ formation is regulated by Cx43-binding molecules. Cx43 binds to the junctional adhesion molecule-associating proteins zonula occludens-1 (ZO-1) and β-catenin.[13,14] Dominant-negative ZO-1, which dissociates the endogenous ZO-1 from Cx43, disturbs the localization of

Original received May 10, 2005; resubmission received July 12, 2005; revised resubmission received August 11, 2005; accepted August 16, 2005.

From the Department of Structural Analysis (S.F., Y.N., H.F., N.M.), National Cardiovascular Center Research Institute, Suita, Osaka; the First Department of Internal Medicine (S.S., Y.S.), Nara Medical University, Kashihara, Nara, Japan.

Correspondence to Naoki Mochizuki, Department of Structural Analysis, National Cardiovascular Center Research Institute, 5-7-1 Fujishirodai, Suita, Osaka 565-8565, Japan. E-mail nmochizu@ri.ncvc.go.jp

Circulation Research **is available at http://circres.ahajournals.org** **DOI: 10.1161/01.RES.0000183880.49270.f9**

Cx43 at the cell–cell contacts, resulting in the reduced conductance of GJs.[13] Wnt-1 signal prevents β-catenin degradation, thereby increasing β-catenin, which not only drives Cx43 expression but also associates with the Cx43 at the cell–cell contacts, where β-catenin localizes with cadherin.[14]

cAMP-induced Cx43 assembly has been extensively characterized in terms of Cx43 synthesis, delivery to the plasma membrane, and phosphorylation, which is believed to depend exclusively on PKA.[15] However, other downstream molecules of cAMP have not been elucidated in the neoformation of GJs. We and others have demonstrated that exchange protein directly activated by cAMP (Epac)/cAMP-GEF, a guanine nucleotide exchange factor (GEF) for Rap1, is activated by cAMP,[16,17] and that cAMP–Epac-Rap1 signal enhances the barrier function of vascular endothelial cells by stabilizing cadherin-mediated cell adhesion.[18,19] Analogous to this Epac-induced cadherin-based cell adhesion, we hypothesized that Epac may be involved in GJ neoformation as a cAMP-triggered signaling molecule in cardiac myocytes.

In this study, we investigated the molecular mechanism by which GJ neoformation is regulated by cAMP using a PKA-specific activator and an Epac-specific activator. We analyzed the GJ accumulation at cell–cell contacts by immunostaining of Cx43 and the gating function of GJs by dye spreading in neonatal rat cardiomyocytes (NRCMs) stimulated with these activators. We demonstrate that the Cx43 accumulation at cell–cell contacts depends on Epac and that dye spreading depends on PKA. Therefore, PKA and Epac downstream of cAMP cooperatively enhance functional GJ neoformation in cardiac myocytes.

Materials and Methods

Reagents and cAMP Analogs

Dibutyryl-cAMP (dbcAMP) was purchased from Sigma-Aldrich, Epac-specific activator 8-(4-chlorophenylthio)-2′-*O*-methyladenosine-3′,5′-cyclic monophosphate (8CPT) from Calbiochem; and PKA-specific activator N^6-benzoyladenosine-3′,5′-cyclic monophosphate (6Bnz) was from BIOLOG Life Science Institute. Other chemical compounds, antibodies, and adenoviruses are listed in the supplemental information (available online at http://circres.ahajournals.org).

Cell Culture

NRCMs were isolated from Wistar rats (1 to 2 days old; Kiwa Jikken Dobutsu, Japan) on a Percoll gradient as described previously.[20] The details of cardiac myocyte preparation are described in the supplemental information. The NRCMs spread onto the glass-base dishes for 24 hours after isolation were subjected to immunostaining or dye transfer assay after drug treatment for another 12 hours. We observed that the adherens junctions (AJs) were not maturated, although NRCMs contacted each other before the drug treatment, indicating that we used the reassembling NRCMs for the experiments. Experiments using animals were approved by our institutional animal use and care committee. All animal procedures were performed according to the *Guide for the Care and Use of Laboratory Animals* (NIH, revision 1996).

Immunocytochemistry

NRCMs stimulated with cAMP analogs were immunostained as described previously.[21] Briefly, cells cultured on glass-base dish were blocked with PBS containing 4% BSA for 1 hour at room temperature (RT), then stained with anti-Cx43, anti–sarcomeric α-actinin (S-αA), and anti–neural (N)-cadherin at RT. Protein reacting with primary antibodies was visualized with Alexa 488–labeled goat anti-rabbit IgG and Alexa 546–labeled goat anti-mouse IgG. Images were recorded with a confocal microscope (BX50WI; Olympus). For quantitative immunofluorescence analysis, images were also recorded using an epifluorescence microscope (IX-71; Olympus) controlled by MetaMorph version 6.2 software (Molecular Devices). The number of Cx43-positive dots at the cell–cell contacts on the fluorescence images were counted as Cx43 puncta.

Gating Function of GJs Analyzed by Microinjected Dye Transfer

Microinjected dye transfer was performed as described by Doble et al, with minor modifications.[22] The details of dye transfer method are described in the supplemental information.

RT-PCR Analysis

Total RNAs extracted from NRCMs and human cervical carcinoma cell line (HeLa) cells using Trizol (Invitrogen) were reverse-transcribed using SuperScript II and random primers (Invitrogen). The resultant DNAs were PCR-amplified using Epac-specific primers described in the supplemental information.

Western Blot Analysis and N-Cadherin Translocation Assay

NRCMs were lysed in buffer described in the supplemental information. Lysates precleared by centrifugation at 15 000*g* for 10 minutes were subjected to SDS-PAGE and immunoblotting with antibodies as indicated in Figures 3, 4, 5, and 6. Proteins reacting with primary antibodies were visualized by an enhanced chemiluminescence system (Amersham Biosciences) with peroxidase-conjugated and species-matched secondary antibodies and analyzed with an LAS-1000 system (Fuji Film). N-cadherin translocation assay was performed as described previously.[18]

Detection of GTP-Bound Form of Rap1

Rap1 activity was assessed by a modified Bos method as described previously.[23] Briefly, NRCMs starved in DMEM for 3 hours were treated with the stimulants as indicated in Figures 3 and 6 and lysed at 4°C in a pull-down lysis buffer described in the supplemental information. GTP-bound Rap1 was collected on glutathione *S*-transferase fused with Rap1 binding domain of Ral guanine nucleotide dissociation stimulator precoupled to glutathione-Sepharose beads and subjected to SDS-PAGE followed by immunoblotting using anti-Rap1.

Statistical Analysis

The results were expressed as the mean±SD. Student *t* test was used to analyze differences between two groups. Group differences were assessed with one-way ANOVA or two-way ANOVA, followed by post hoc comparisons tested with Scheffe's method. At least 3 fields randomly selected from each culture for analysis of Cx43 staining or at least 4 cells for dye transfer assay from each culture were used to yield a single value for each culture. The number of the cultures for analysis was indicated in the figure legends as n. Significant differences were indicated as P value <0.05 (*).

Results

cAMP Enhances Functional GJ Neoformation in Cultured NRCMs

Because cAMP has been reported previously to enhance GJ formation,[7] we confirmed the dbcAMP–regulated functional GJ neoformation by quantitatively analyzing Cx43 accumulation at the cell–cell contacts by immunostaining and gating function of GJs by microinjected dye transfer assay. dbcAMP enhanced the Cx43 accumulation at the cell–cell contacts (Figure 1A and 1B). To neglect the possibility of cardiac fibroblast contamination in the NRCMs in the following

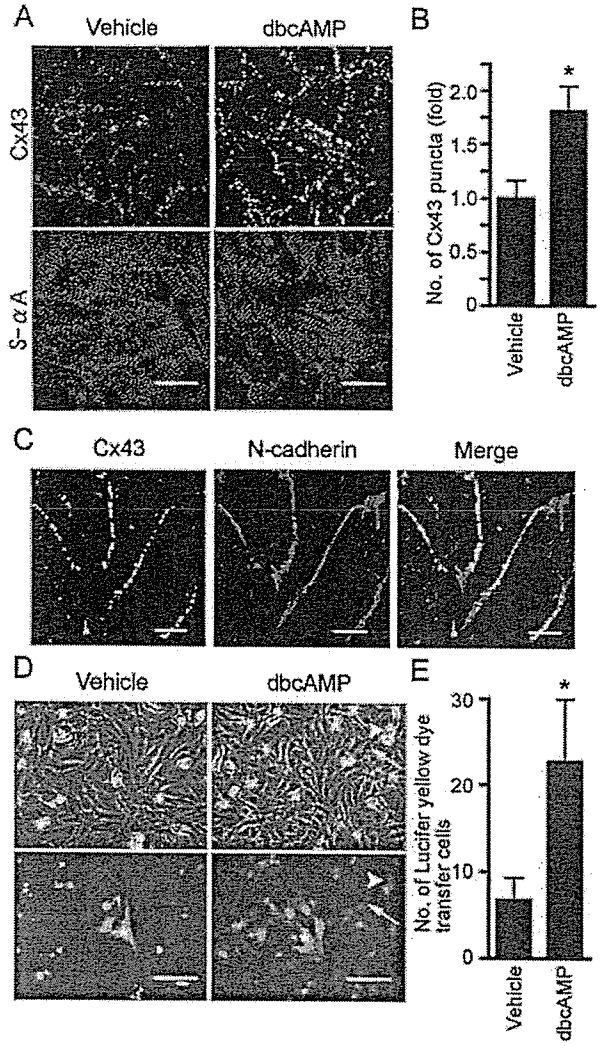

Figure 1. cAMP induces Cx43 accumulation at cell–cell contacts and enhances gap junctional intercellular communication. A, NRCMs cultured 24 hours after cell preparation were stimulated with vehicle or 1 mmol/L dbcAMP for 12 hours. Cells were stained with anti-Cx43 (green) and anti-S-αA (red). Images were obtained through a confocal microscope (BX50WI). Bar=20 μm. B, NRCMs stimulated by dbcAMP were analyzed for Cx43 accumulation by counting the number of puncta at cell–cell contacts. Mean number±SD is expressed as fold increase relative to that observed in the cell treated with vehicle. *$P<0.05$ vs vehicle as analyzed by Student's t test (n=4). Three fields randomly selected from each culture were used for measuring the fold activation between vehicle- and dbcAMP-treated culture by counting Cx43-positive puncta. C, Cells treated with dbcAMP were immunostained with anti-Cx43 (green) and anti-N-cadherin (red). A merged image is shown on the right. Note that puncta for Cx43 are localized to cell–cell contacts as indicated by the N-cadherin immunostaining. Bar=5 μm. D, Microinjected dye transfer assay shows the extent of dye transferring between neighboring cells through GJs. NRCMs stimulated with 1 mmol/L dbcAMP for 12 hours were microinjected with 10% Lucifer yellow. Cells 3 minutes after dye injection were phase contrast imaged (top panels) and fluorescence imaged (bottom panels). Asterisks indicate dye-injected cells. Arrows and arrowheads denote typical dye-transferred cell and cell debris emitting nonspecific fluorescence, respectively. Bar=50 μm. E, Quantitative analysis of D is shown as mean number of dye-positive cells in either vehicle or dbcAMP-treated NRCMs. *$P<0.05$ as analyzed by Student's t test (n=6).

experiments, and to show the confluence of the NRCMs, cells were immunostained for sarcomeric α-actinin (Figure 1A, bottom). The Cx43 puncta in the cells treated with dbcAMP for 12 hours were clearly observed at the cell–cell contacts, where N-cadherin localized (Figure 1C), indicating that dbcAMP induces the accumulation of Cx43 at the cell–cell contacts. We investigated the effect of dbcAMP on gating function of GJs by microinjected dye transfer assays (Figure 1D and 1E). Microinjected dye was more widely transferred to the neighboring cells in dbcAMP-treated NRCMs than vehicle-treated cells (Figure 1D). The quantitative data are shown in Figure 1E. These results are in agreement with previous reports[7,8] and validated the assays we used in this study.

PKA Is Required But Not Sufficient Alone for cAMP-Enhanced GJ Neoformation

Because PKA is involved in the enhancement of GJ formation,[15] we first tested the effect of H89, a specific PKA inhibitor, on cAMP-enhanced accumulation of Cx43. Unexpectedly, H89 did not block the dbcAMP-induced accumulation of Cx43 (Figure 2A and 2B), although H89 did block cAMP-enhanced intercellular communication assessed by microinjected dye transfer assays (Figure 2C).

We next examined the effect of 6Bnz, a specific activator for PKA,[24] on intercellular communication and Cx43 accumulation at cell–cell contacts to directly assess the involvement of PKA in cAMP-enhanced GJ formation. 6Bnz induced Cx43 accumulation slightly but to a much lesser extent than dbcAMP (Figure 2D and 2E). Notably, 6Bnz enhanced dye transfer to a greater extent than vehicle but to a lesser extent than dbcAMP (Figure 2F). These results indicate that PKA signaling is required but not sufficient alone for cAMP-enhanced GJ neoformation and suggest that there is a novel signaling downstream of cAMP in addition to PKA involved in Cx43 accumulation at cell–cell contacts for functional GJ neoformation.

cAMP Activates PKA and Epac-Rap1 Signaling in NRCMs

Epac has been identified as a novel cAMP target and a Rap1-specific GEF. We therefore hypothesized that Epac-Rap1 signaling may be involved in cAMP-enhanced GJ neoformation. RT-PCR analysis revealed the expression of Epac in NRCM but not in HeLa cells used as a negative control (Figure 3A). To test the hypothesis, we first examined whether dbcAMP induces the activation of Rap1 and the phosphorylation of cAMP response element binding protein (CREB) in NRCMs. As shown in Figure 3B, dbcAMP induced Rap1 and CREB activation in NRCMs. Rap1 activation by dbcAMP is dependent on time and concentration (supplemental Figure IA and IB, available online at http://circres.ahajournals.org). H89 inhibited dbcAMP-induced CREB phosphorylation but not dbcAMP-induced Rap1 activation (Figure 3B and 3C), indicating that Rap1 activation does not depend on PKA, whereas CREB phosphorylation depends exclusively on PKA. We next tested whether Rap1 activation and CREB phosphorylation are induced by 8CPT, which has been developed recently as a specific activator for Epac.[25] 8CPT only activated Rap1, not CREB. In striking contrast, 6Bnz induced CREB activation but did not affect

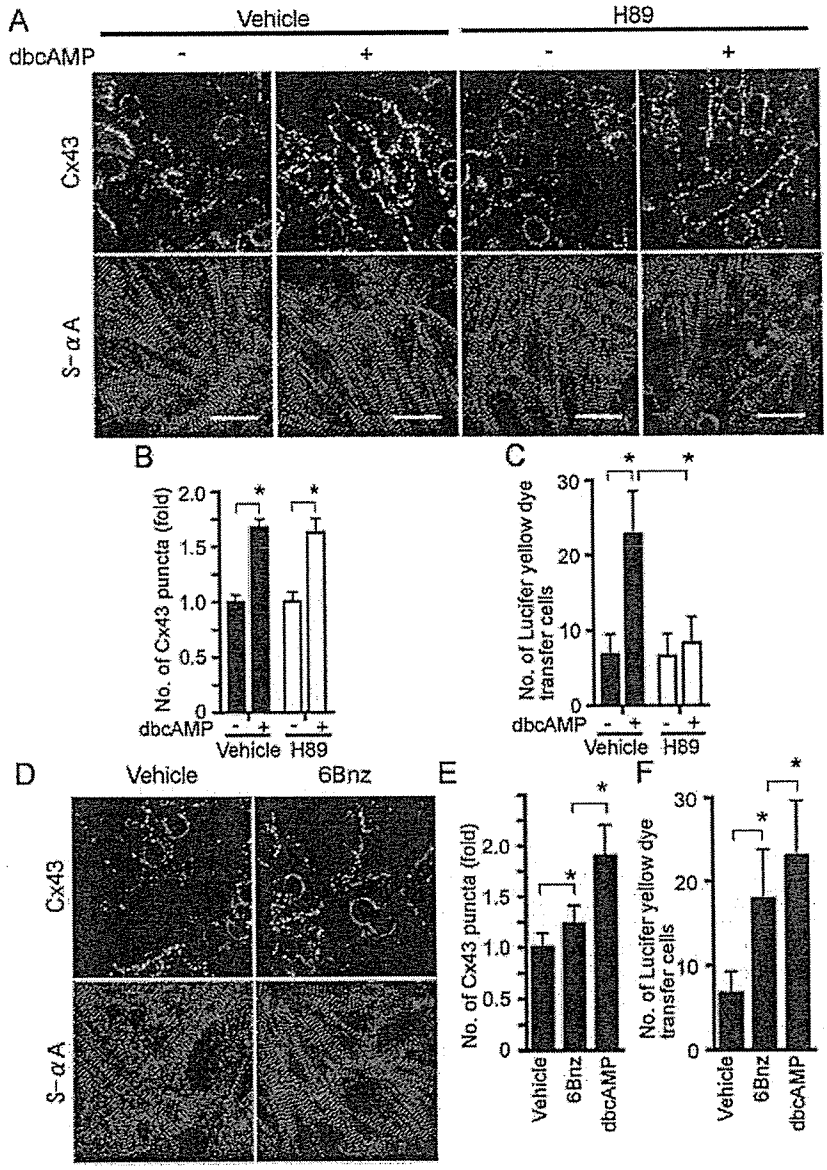

Figure 2. PKA signaling mainly contributes to gating function of GJs. A, NRCMs pretreated with or without 5 μmol/L H89 for 30 minutes were stimulated with or without 1 mmol/L dbcAMP in the presence or absence of 5 μmol/L H89 for 12 hours. After the stimulation, cells were immunostained with anti-Cx43 and anti-S-αA as described in Figure 1A legend. Bar=20 μm. B, Cx43 accumulation in cells treated as in A was quantitatively analyzed. Statistical significance between groups was analyzed by two-way ANOVA with Scheffe's method, indicating that the factor of with/without dbcAMP is significant but not that of vehicle/H89 (*P<0.05; n=6) C, Effect of H89 on dbcAMP-enhanced gap junctional intercellular communication was evaluated by microinjected dye transfer assay as described in Figure 1E legend. Statistical significance between groups was analyzed by two-way ANOVA with Scheffe's method, indicating that both factors, with/without dbcAMP and vehicle/H89, are significant (*P<0.05; n=6). D, NRCMs were stimulated with either vehicle or 1 mmol/L 6Bnz for 12 hours and immunostained with anti-Cx43 and anti-S-αA. Bar=20 μm. E, The effect of 1 mmol/L 6Bnz on Cx43 accumulation at the cell–cell contacts was evaluated similarly to Figure 1B. Statistical significance between groups was analyzed by one-way ANOVA with Scheffe's method (*P<0.05; n=4). F, The effect of 6Bnz on junctional intercellular communication between NRCMs was similarly evaluated by microinjected dye transfer assay to the Figure 1D. Statistical significance was evaluated by one-way ANOVA with Scheffe's method (*P<0.05; n=4).

Rap1 activity (Figure 3D and 3E). Together, these findings demonstrate that cAMP activates Epac-Rap1 and PKA signaling pathways in NRCMs.

Activation of Epac Signaling Leads to Cx43 Accumulation at Cell–Cell Contacts

Because we observed Rap1 activation in response to dbcAMP, we proceeded to investigate the involvement of Epac-Rap1 signaling in cAMP-induced Cx43 accumulation at cell–cell contacts. Like dbcAMP, 8CPT significantly enhanced the accumulation of Cx43 at the cell–cell contacts (Figure 4A and 4B). 8CPT induced Cx43 accumulation at the cell–cell contacts to a similar extent to dbcAMP and to a greater extent than 6Bnz. 6Bnz only slightly increased the number of Cx43 puncta (Figure 4B) compared with vehicle and did not further increase the accumulation of Cx43 at cell–cell contacts caused by 8CPT alone. These results indicate that Epac-mediated signaling is mainly responsible for cAMP-induced Cx43 accumulation at the cell–cell contacts.

We excluded the possibility that increased synthesis of Cx43 on cAMP stimulation resulted in the accumulation of Cx43 at the cell–cell contacts. No discernible increase was observed in the cells stimulated with vehicle, dbcAMP, 8CPT, 6Bnz, and a combination of 8CPT and 6Bnz for 12 hours (Figure 4C and 4D), suggesting that distribution or functional augmentation of GJs is essential for cAMP-induced functional GJ neoformation. In addition, phosphorylation of Cx43 was not affected by dbcAMP, 8CPT, or 6Bnz, nor a combination of 8CPT and 6Bnz (Figure 4C and 4E).

Epac Enhances AJ Formation

Several lines of evidence suggest that AJ formation organized by N-cadherin is a prerequisite for GJ assembly in cardiomyocytes when reassembling and recoupling.[26–28] We used reassembling NRCMs before drug treatment. Recently, we and others revealed that Rap1 is involved in the cell–cell contacts mediated by epithelial (E)-cadherins and vascular

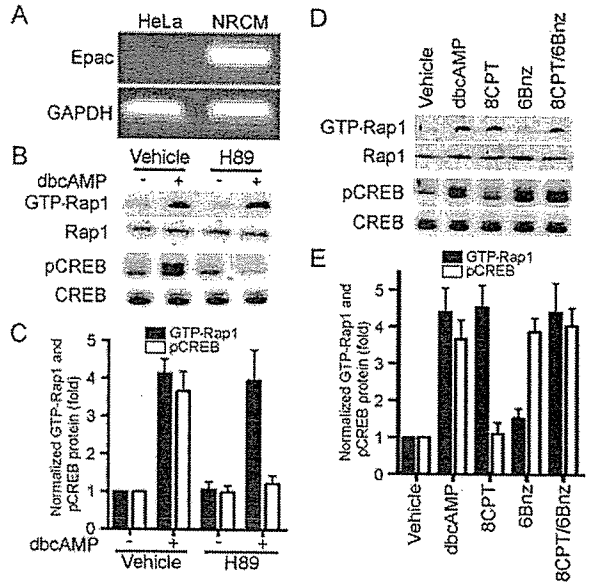

Figure 3. cAMP induces Epac-Rap1 signal as well as PKA signal in NRCMs. A, RT-PCR analysis shows the expression of Epac in NRCMs but not in HeLa cells (used as a negative control). GAPDH was shown as a positive control for RT-PCR. B, Serum-starved NRCMs were stimulated with 1 mmol/L dbcAMP in the absence or presence of H89 for 15 minutes. GTP-bound Rap1 were assessed by pull-down assay. Phosphorylation of CREB was analyzed by Western blot analysis using anti-CREB and anti-phospho-CREB (pCREB). A representative result of 3 independent experiments is shown. C, Data obtained from 4 independent experiments were analyzed quantitatively. Fold activation indicates the ratio of the poststimulation GTP-Rap1 and pCREB intensity of total Rap1 and CREB intensity to the prestimulation GTP-Rap1 and pCREB intensity of total Rap1 and CREB intensity. D, Serum-starved NRCMs were stimulated with either vehicle, 1 mmol/L dbcAMP, 1 mmol/L 8CPT, 1 mmol/L 6Bnz, or 1 mmol/L 8CPT and 1 mmol/L 6Bnz for 15 minutes. GTP-bound Rap1 and phosphorylation of CREB were assessed as described in B. E, Data obtained from 4 independent experiments were analyzed similarly to C.

endothelial–cadherins (VE-cadherins).[18,29] Thus, it is possible that cAMP enhances GJ neoformation by enhancing N-cadherin–mediated AJ formation preceding the GJ formation in NRCMs. To address this possibility, we investigated whether cAMP induces N-cadherin–mediated AJ formation in NRCMs. N-cadherin distribution at cell–cell contacts was enhanced by dbcAMP and 8CPT, whereas 6Bnz neither affected the distribution of N-cadherin nor enhanced the effect of 8CPT (Figure 5A).

To quantitatively analyze the localization of N-cadherin after drug treatment, we performed a biochemical N-cadherin translocation assay. Because N-cadherin is connected to actin cytoskeleton in maturated AJs, cadherin anchored to actin cytoskeleton can be detected in detergent-insoluble fractions of cell lysates. We found an increase in N-cadherin in Triton X-100–insoluble fraction when stimulated by dbcAMP and 8CPT (Figure 5B). However, 6Bnz did not change either basal- or 8CPT-increased levels of N-cadherin in the Triton X-100–insoluble fraction (Figure 5B and 5C). Collectively, these findings indicate that cAMP enhances AJ formation through Epac in NRCMs. We found no difference in N-cadherin expression in NRCMs stimulated with dbcAMP, 8CPT, or 6Bnz, or a combination of 8CPT and 6Bnz by immunoblotting (data not shown).

Rap1 Activation Is Essential for cAMP-Mediated Cx43 Redistribution and AJ Formation

We investigated the role of Rap1 in cAMP-induced Cx43 accumulation and AJ formation in NRCMs. To examine the effect of Rap1 on AJ and GJ formation, we inactivated Rap1 by adenovirus-expressing Rap1GAP1b, which specifically catalyzes the hydrolysis of GTP to GDP on Rap1.[30] Endogenous Rap1 activity was almost completely suppressed by the expression of increasing amount of Rap1GAP1b in NRCMs (Figure 6A). Moreover, overexpression of Rap1GAP1b inhibited cAMP-induced Rap1 activity without affecting cAMP-stimulated CREB phosphorylation (Figure 6B), confirming that Rap1GAP1b specifically blocks Epac-Rap1 pathway but not PKA-mediated signaling.

Inactivation of Rap1 blocked the cAMP-induced accumulation of Cx43 and N-cadherin at the cell–cell contacts (Figure 6C and 6D). dbcAMP-induced translocation of N-cadherin to cytoskeleton-anchored fraction was inhibited by inactivation of Rap1 but not by LacZ overexpression (Figure 6E and 6F). These results suggest that cAMP induces N-cadherin–based AJ assembly through an Epac-Rap1 signaling pathway, which may precede the accumulation of Cx43-based GJs.

PKA and Epac-Rap1 Signaling Cooperatively Enhances GJ Neoformation in NRCMs

Because we found that PKA alone is not sufficient for cAMP-enhanced GJ neoformation and that Epac-Rap1 signaling is involved in cAMP-induced accumulation of Cx43, we assessed the effect of PKA activation and Epac-Rap1 activation on gating function of GJs. 8CPT merely showed the weak enhancement of the intercellular connection, as revealed by microinjected dye transfer assay (Figure 7A). However, 8CPT significantly enhanced 6Bnz-mediated intercellular communication (Figure 7B). The effect of the combination of 8CPT and 6Bnz was comparable to that of dbcAMP. Given that 8CPT induces the Cx43 accumulation at the cell–cell contacts, cAMP potentiates functional GJ neoformation via a PKA-mediated enhanced gating function and Epac-Rap1 signal-mediated accumulation of Cx43 to cell–cell contacts.

Discussion

The function of GJs in the heart depends on the number of GJs between neighboring cells and the gating function of individual GJ at the cell–cell contacts. We investigated how cAMP induces Cx43 accumulation at cell–cell contacts and enhances gating function in NRCMs that were about to develop the mature cell–cell contacts. For the first time, we demonstrated the involvement of Epac-Rap1 signaling downstream of cAMP in GJ neoformation of cardiomyocytes. Although Cx43 accumulated at the cell–cell contacts on cAMP stimulation has been ascribed to PKA,[7] this study demonstrated that Epac-Rap1 signaling activated by cAMP is mainly responsible for the redistribution of Cx43 to cell–cell contacts.

The number of GJs was increased by Epac-Rap1 downstream of cAMP as indicated by the increase in Cx43-positive puncta at cell–cell contacts. However, there was no increase in the amount of Cx43 after cAMP treatment, indicating the importance of the redistribution of Cx43 rather than increase of Cx43 transcription on cAMP. How does Epac signaling induce the accumulation of Cx43 at cell–cell contacts?

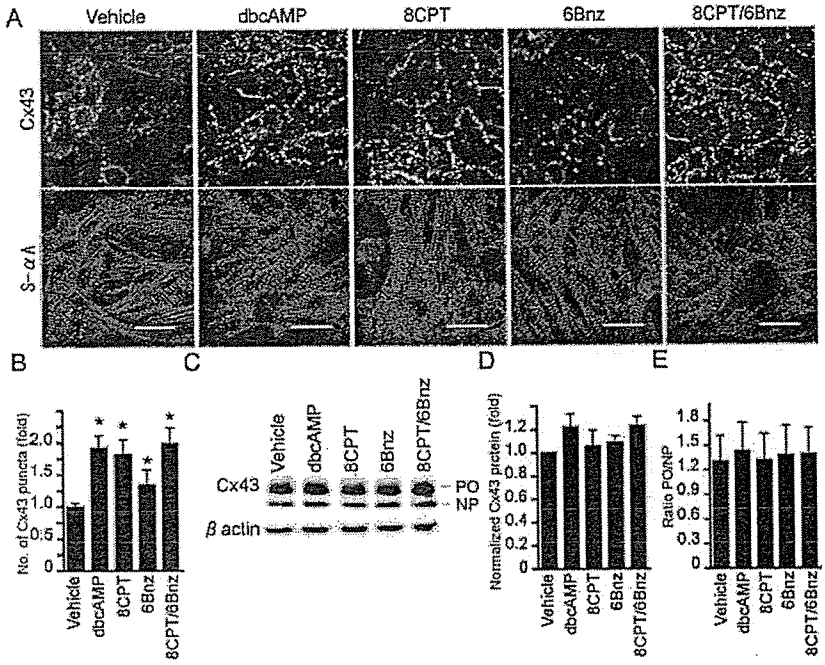

Figure 4. Activation of Epac signaling induces Cx43 accumulation at cell–cell contacts. A, NRCMs stimulated for 12 hours with drugs as indicated at the top were stained with anti-Cx43 and anti-S-αA as described in Figure 1A legend. Bar=20 μm. B, Cx43 accumulation was quantitatively analyzed in Figure 1B. Significant differences between vehicle-treated cells and all drug-treated cells was analyzed by one-way ANOVA with Scheffe's method (*$P<0.05$; n=6). C, NRCMs stimulated as indicated at the top were examined for Cx43 by Western blot analysis. Upper and lower bands correspond to phosphorylated (PO) and nonphosphorylated (NP) Cx43, respectively. D, Total Cx43 (phosphorylated and nonphosphorylated) expression of NRCMs treated for 12 hours with drugs as indicated at the bottom was quantitatively analyzed by three independent Western blot analyses for Cx43. The intensity of the drug-stimulated Cx43 normalized by β-catenin divided by that of vehicle-stimulated Cx43 was expressed as fold activation. E, The ratio is expressed by the intensity of phosphorylated Cx43 (PO) divided by that of nonphosphorylated Cx43 (NP).

Epac-Rap1 activation resulted in enhancement of AJ formation accompanied by GJ formation, as evidenced by increases in N-cadherin and Cx43 at the cell–cell contacts after dbcAMP stimulation (Figure 5). AJ formation constituted by N-cadherin is a prerequisite for GJ neoformation.[28,31] When adult myocytes are cultured, Cx43 is transported and accumulated at the plasma membrane, where N-cadherin accumulates on cell–cell contact.[26] Therefore, GJ formation depends on N-cadherin–based AJ maturation. We have shown previously that the Epac-Rap1 signal enhances the VE-cadherin–based cell–cell contacts in vascular endothelial cells.[18] In this study, we found that Epac activation resulted in the increased accumulation of N-cadherin at the intercellular junction of NRCMs. Thus, N-cadherin accumulation at the cell–cell contacts induced by the Epac-Rap1 signal may account for Cx43 accumulation in NRCMs by analogy to Epac-Rap1–triggered VE-cadherin accumulation in vascular endothelial cells.

The target of activated Rap1 for enhancement of cadherin-based AJ is still unclear. Rac belonging to Rho family GTPase and regulating actin cytoskeleton is suggested to function downstream of Rap1.[32] Therefore, Rac may increase the chances of cell contacts and induce cadherin engagement by extending membrane downstream of Rap1. Maturated N-cadherin on Epac activation, which is detected in the cytoskeleton-anchored fraction, may be accompanied by translocation of Cx43 through cadherin-associating β-catenin

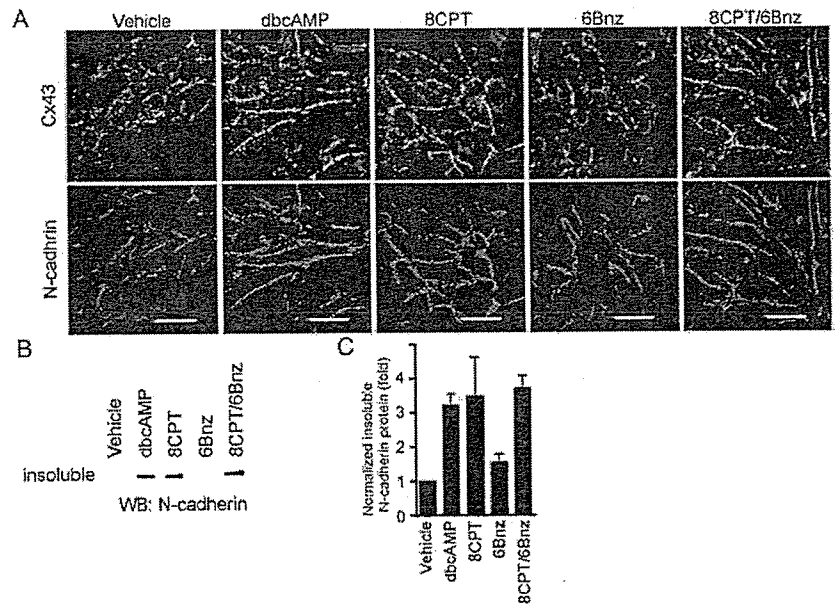

Figure 5. Activation of Epac induces AJ formation. A, NRCMs stimulated for 12 hours with drugs as indicated at the top were immunostained with anti-Cx43 (green) and anti–N-cadherin (red). Bar=20 μm. B, NRCMs stimulated as in A were fractionated with cytoskeleton stabilizing buffer. Triton X-100–insoluble fraction was subjected to SDS-PAGE followed by Western blot analysis (WB) with anti–N-cadherin. A representative result of three independent experiments is shown. C, The data obtained from three independent experiments of B was quantitatively analyzed. The result is indicated as fold increase calculated by dividing the amount of insoluble N-cadherin from the cells treated with the drug by that from the cells treated with vehicle.

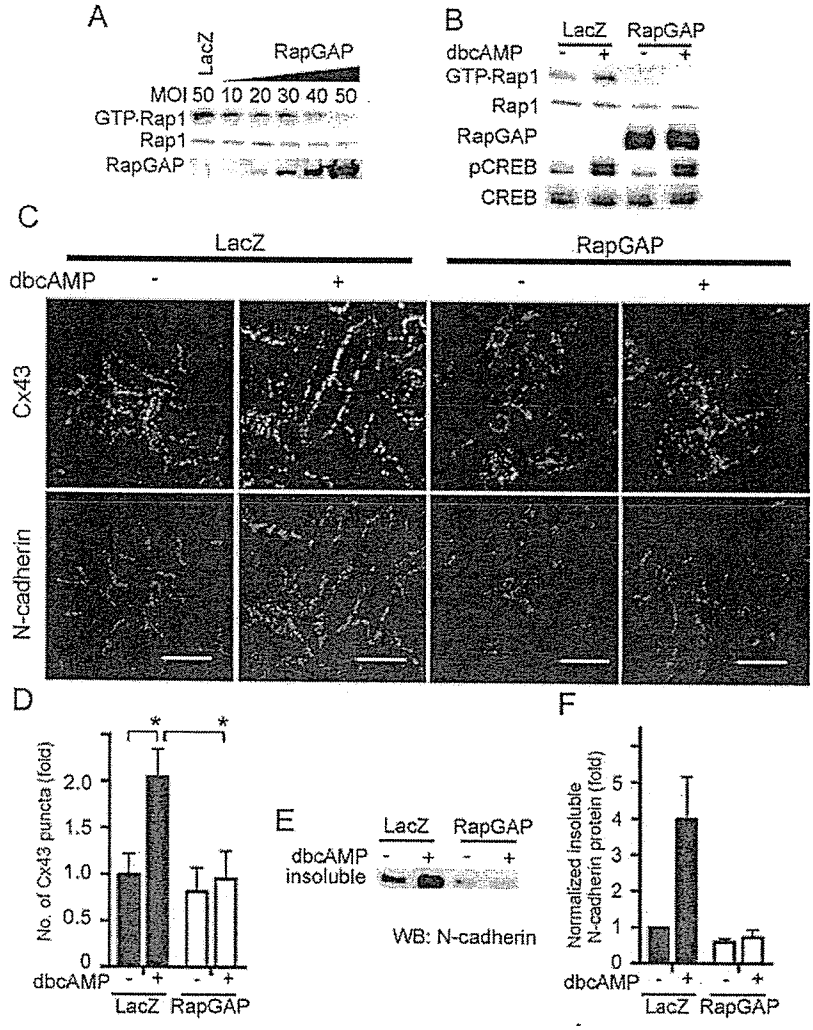

Figure 6. Rap1 activation is required for cAMP-induced Cx43 accumulation at the cell–cell contacts and AJ formation. A, Rap1 inactivation by Rap1GAP1b was verified by detecting GTP-Rap1 in NRCMs infected with different multiplicity of infection (MOI) of adenovirus-expressing Rap1GAP1b (Ad-RapGAP). An adenovirus-expressing LacZ (Ad-LacZ) at 50 MOI was used as a control. GTP-Rap1 was detected by pull-down assay. Rap1 and Rap1GAP1b (RapGAP) expression was examined by Western blot analysis using antibodies as indicated at the left. B, NRCMs infected with either Ad-LacZ or Ad-RapGAP at an MOI of 50 for 24 hours were stimulated with vehicle (−) or 1 mmol/L dbcAMP (+) for 15 minutes and analyzed for Rap1 and CREB activation. C, Localization of N-cadherin and Cx43 was examined similarly to Figure 5A in NRCMs infected with Ad-LacZ or Ad-RapGAP after stimulated with vehicle or 1 mmol/L dbcAMP for 12 hours. Bar=20 μm. D, The effect of inactivation of Rap1 on dbcAMP-induced accumulation of Cx43 was analyzed by two-way ANOVA with Scheffe's method, indicating that both factors, with/without dbcAMP and LacZ/RapGAP, are significant (*P<0.05; n=6). E, Translocation of N-cadherin was examined in NRCMs infected with Ad-LacZ or Ad-RapGAP after stimulation of dbcAMP. A representative of three independent results is shown. F, The three independent results from D were analyzed similarly to Figure 5C.

because Cx43 is capable of binding to β-catenin.[14] Because ZO-1 is recruited to AJs by binding to α-catenin and is also capable of binding to Cx43,[33] ZO-1 may participate in the accumulation of Cx43 during maturation of AJs.

Another factor affecting functional GJ neoformation in addition to the number of GJs is the gating function of individual GJs. PKA activation facilitates intercellular communication without accumulation of Cx43 at cell–cell contacts, concurring with previous reports underpinning that PKA and cAMP increases single channel conductance of the GJ,[34] although the characteristics of single GJ channel conductance evoked by PKA activation still remains elusive.[15]

We found a marked increase in dye transfer on PKA activation with a slightly increased accumulation of Cx43 at the cell–cell contacts (Figures 4 and 7). These results indicate that PKA mainly contributes to the functional neoformation of GJs by enhancing gating function of GJs. Phosphorylation of Cx43 on Ser residues is required for intercellular communication of GJs.[35] Because we found no significant increase in either total Cx43 or phosphorylated Cx43, PKA may indirectly modulate GJ conductance in addition to direct phosphorylation of Cx43 or may phosphorylate a critical Ser/Thr that was indistinguishable in the phosphorylated Cx43 band in our immunoblot for Cx43 (Figure 4C).

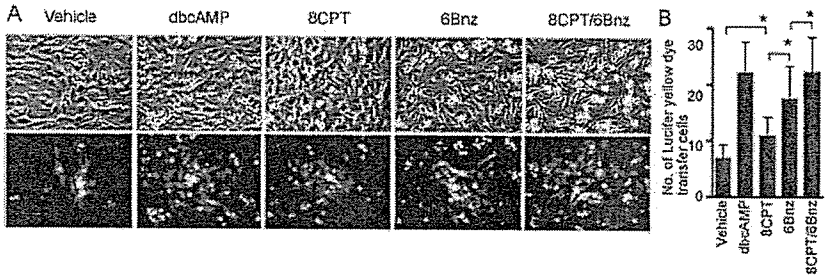

Figure 7. PKA signal and Epac-Rap1 signal cooperatively enhance intercellular communication through GJs. A, Intercellular communication was assessed by microinjected dye transfer assay using NRCMs stimulated with drugs as indicated at the top. B, Dye spread was quantitatively analyzed similarly to Figure 2F. Statistical significance between groups was evaluated by one-way ANOVA with Scheffe's method (*P<0.05; n=6).

The enhanced gating function of GJs is mainly ascribed to PKA, whereas the accumulation of Cx43 to cell–cell contacts is mainly attributable to Epac-Rap1 signal. Hence, Epac-Rap1 signal may accelerate the trafficking of Cx43 to the plasma membrane or inhibit the endocytosis of Cx43 from the plasma membrane. We did not quantify the translocation of Golgi fraction to cell–cell contacts on cAMP stimulation. Previously, GJ trafficking was dynamically monitored by green fluorescence protein–tagged Cx43.[36] Therefore, it will be of great interest to observe the Cx43 dynamics on 8CPT stimulation to directly elucidate Epac-Rap1 signaling.

In conclusion, we demonstrated that cAMP potentiates functional GJ neoformation by a PKA-dependent increase in intercellular communication and by an Epac-Rap1–dependent accumulation of Cx43 in NRCMs.

Acknowledgments

This work was supported in part by grants from the Ministry of Health, Labor, and Welfare Foundation of Japan; the Ministry of Education, Science, Sports, and Culture of Japan; the Promotion of Fundamental Studies in Health Science of the Organization for Pharmaceutical Safety and Research of Japan; the Japan Health Science Foundation; and Astellas Foundation for Research on Metabolic Disorders. We thank Michiyuki Matsuda and Akihiro Umezawa for their helpful input; Nobuo Shirahashi for statistical analysis; James T. Pearson and Michael E. Mendelsohn for critical reading; and Yuko Matsuura and Manami Sone for their technical assistance.

References

1. Yeager M. Structure of cardiac gap junction intercellular channels. *J Struct Biol.* 1998;121:231–245.
2. Sohl G, Willecke K. Gap junctions and the connexin protein family. *Cardiovasc Res.* 2004;62:228–232.
3. Vozzi C, Dupont E, Coppen SR, Yeh HI, Severs NJ. Chamber-related differences in connexin expression in the human heart. *J Mol Cell Cardiol.* 1999;31:991–1003.
4. Davis LM, Rodefeld ME, Green K, Beyer EC, Saffitz JE. Gap junction protein phenotypes of the human heart and conduction system. *J Cardiovasc Electrophysiol.* 1995;6:813–822.
5. Saffitz JE, Kleber AG. Effects of mechanical forces and mediators of hypertrophy on remodeling of gap junctions in the heart. *Circ Res.* 2004;94:585–591.
6. Gutstein DE, Morley GE, Fishman GI. Conditional gene targeting of connexin43: exploring the consequences of gap junction remodeling in the heart. *Cell Commun Adhes.* 2001;8:345–348.
7. Darrow BJ, Fast VG, Kleber AG, Beyer EC, Saffitz JE. Functional and structural assessment of intercellular communication. Increased conduction velocity and enhanced connexin expression in dibutyryl cAMP-treated cultured cardiac myocytes. *Circ Res.* 1996;79:174–183.
8. Paulson AF, Lampe PD, Meyer RA, TenBroek E, Atkinson MM, Walseth TF, Johnson RG. Cyclic AMP and LDL trigger a rapid enhancement in gap junction assembly through a stimulation of connexin trafficking. *J Cell Sci.* 2000;113:3037–3049.
9. Saffitz JE, Laing JG, Yamada KA. Connexin expression and turnover: implications for cardiac excitability. *Circ Res.* 2000;86:723–728.
10. Lampe PD, TenBroek EM, Burt JM, Kurata WE, Johnson RG, Lau AF. Phosphorylation of connexin43 on serine368 by protein kinase C regulates gap junctional communication. *J Cell Biol.* 2000;149:1503–1512.
11. TenBroek EM, Lampe PD, Solan JL, Reynhout JK, Johnson RG. Ser364 of connexin43 and the upregulation of gap junction assembly by cAMP. *J Cell Biol.* 2001;155:1307–1318.
12. Lin R, Warn-Cramer BJ, Kurata WE, Lau AF. v-Src phosphorylation of connexin 43 on Tyr247 and Tyr265 disrupts gap junctional communication. *J Cell Biol.* 2001;154:815–827.
13. Toyofuku T, Yabuki M, Otsu K, Kuzuya T, Hori M, Tada M. Direct association of the gap junction protein connexin-43 with ZO-1 in cardiac myocytes. *J Biol Chem.* 1998;273:12725–12731.
14. Ai Z, Fischer A, Spray DC, Brown AM, Fishman GI. Wnt-1 regulation of connexin43 in cardiac myocytes. *J Clin Invest.* 2000;105:161–171.
15. Schulz R, Heusch G. Connexin 43 and ischemic preconditioning. *Cardiovasc Res.* 2004;62:335–344.
16. Kawasaki H, Springett GM, Mochizuki N, Toki S, Nakaya M, Matsuda M, Housman DE, Graybiel AM. A family of cAMP-binding proteins that directly activate Rap1. *Science.* 1998;282:2275–2279.
17. de Rooij J, Zwartkruis FJ, Verheijen MH, Cool RH, Nijman SM, Wittinghofer A, Bos JL. Epac is a Rap1 guanine-nucleotide-exchange factor directly activated by cyclic AMP. *Nature.* 1998;396:474–477.
18. Fukuhara S, Sakurai A, Sano H, Yamagishi A, Somekawa S, Takakura N, Saito Y, Kangawa K, Mochizuki N. Cyclic AMP potentiates vascular endothelial cadherin-mediated cell-cell contact to enhance endothelial barrier function through an Epac-Rap1 signaling pathway. *Mol Cell Biol.* 2005;25:136–146.
19. Cullere X, Shaw SK, Andersson L, Hirahashi J, Luscinskas FW, Mayadas TN. Regulation of vascular endothelial barrier function by Epac, a cAMP-activated exchange factor for Rap GTPase. *Blood.* 2005;105:1950–1955.
20. Oyamada Y, Zhou W, Oyamada H, Takamatsu T, Oyamada M. Dominant-negative connexin43-EGFP inhibits calcium-transient synchronization of primary neonatal rat cardiomyocytes. *Exp Cell Res.* 2002;273:85–94.
21. Ogita H, Kunimoto S, Kamioka Y, Sawa H, Masuda M, Mochizuki N. EphA4-mediated Rho activation via Vsm-RhoGEF expressed specifically in vascular smooth muscle cells. *Circ Res.* 2003;93:23–31.
22. Doble BW, Chen Y, Bosc DG, Litchfield DW, Kardami E. Fibroblast growth factor-2 decreases metabolic coupling and stimulates phosphorylation as well as masking of connexin43 epitopes in cardiac myocytes. *Circ Res.* 1996;79:647–658.
23. Ohba Y, Ikuta K, Ogura A, Matsuda J, Mochizuki N, Nagashima K, Kurokawa K, Mayer BJ, Maki K, Miyazaki J, Matsuda M. Requirement for C3G-dependent Rap1 activation for cell adhesion and embryogenesis. *EMBO J.* 2001;20:3333–3341.
24. Christensen AE, Selheim F, de Rooij J, Dremier S, Schwede F, Dao KK, Martinez A, Maenhaut C, Bos JL, Genieser HG, Doskeland SO. cAMP analog mapping of Epac1 and cAMP kinase. Discriminating analogs demonstrate that Epac and cAMP kinase act synergistically to promote PC-12 cell neurite extension. *J Biol Chem.* 2003;278:35394–35402.
25. Enserink JM, Christensen AE, de Rooij J, van Triest M, Schwede F, Genieser HG, Doskeland SO, Blank JL, Bos JL. A novel Epac-specific cAMP analogue demonstrates independent regulation of Rap1 and ERK. *Nat Cell Biol.* 2002;4:901–906.
26. Hertig CM, Butz S, Koch S, Eppenberger-Eberhardt M, Kemler R, Eppenberger HM. N-cadherin in adult rat cardiomyocytes in culture. II. Spatio-temporal appearance of proteins involved in cell-cell contact and communication. Formation of two distinct N-cadherin/catenin complexes. *J Cell Sci.* 1996;109:11–20.
27. Kostetskii I, Li J, Xiong Y, Zhou R, Ferrari VA, Patel VV, Molkentin JD, Radice GL. Induced deletion of the N-cadherin gene in the heart leads to dissolution of the intercalated disc structure. *Circ Res.* 2005;96:346–354.
28. Kostin S, Hein S, Bauer EP, Schaper J. Spatiotemporal development and distribution of intercellular junctions in adult rat cardiomyocytes in culture. *Circ Res.* 1999;85:154–167.
29. Hogan C, Serpente N, Cogram P, Hosking CR, Bialucha CU, Feller SM, Braga VM, Birchmeier W, Fujita Y. Rap1 regulates the formation of E-cadherin-based cell-cell contacts. *Mol Cell Biol.* 2004;24:6690–6700.
30. Mochizuki N, Ohba Y, Kiyokawa E, Kurata T, Murakami T, Ozaki T, Kitabatake A, Nagashima K, Matsuda M. Activation of the ERK/MAPK pathway by an isoform of rap1GAP associated with G alpha(i). *Nature.* 1999;400:891–894.
31. Volk T, Geiger B. A 135-kDa membrane protein of intercellular adherens junctions. *EMBO J.* 1984;3:2249–2260.
32. Maillet M, Robert SJ, Cacquevel M, Gastineau M, Vivien D, Bertoglio J, Zugaza JL, Fischmeister R, Lezoualc'h F. Crosstalk between Rap1 and Rac regulates secretion of sAPPalpha. *Nat Cell Biol.* 2003;5:633–639.
33. Itoh M, Nagafuchi A, Moroi S, Tsukita S. Involvement of ZO-1 in cadherin-based cell adhesion through its direct binding to alpha catenin and actin filaments. *J Cell Biol.* 1997;138:181–192.
34. De Mello WC. Impaired regulation of cell communication by beta-adrenergic receptor activation in the failing heart. *Hypertension.* 1996;27:265–268.
35. Duncan JC, Fletcher WH. Alpha-1 connexin (connexin43) gap junctions and activities of cAMP-dependent protein kinase and protein kinase C in developing mouse heart. *Dev Dyn.* 2002;223:96–107.
36. Lauf U, Giepmans BN, Lopez P, Braconnot S, Chen SC, Falk MM. Dynamic trafficking and delivery of connexons to the plasma membrane and accretion to gap junctions in living cells. *Proc Natl Acad Sci U S A.* 2002;99:10446–10451.

Journal of Electron Microscopy 54(Supplement 1): i35–i41 (2005)
doi:10.1093/jmicro/dfi006

Crystal structure of troponin and the molecular mechanism of muscle regulation

Soichi Takeda[1,2,*]

[1]Department of Cardiac Physiology, National Cardiovascular Center Research Institute, 5-7-1 Fujishiro-dai, Suita, Osaka 565-8565, Japan and [2]Laboratory of Structural Biochemistry, RIKEN Harima Institute at SPring-8, 1-1-1 Kouto, Mikazuki-cho, Sayo, Hyogo 679-5148, Japan
*E-mail: stakeda@ri.ncvc.go.jp

Abstract — Troponin plays a central role in the regulation of skeletal and cardiac muscle contraction. The protein consists of three polypeptide chains (TnT, TnI and TnC) and is located on polymerized actin together with tropomyosin, forming muscle thin filament. We have determined the molecular structures of the core domains (relative molecular mass of 46 000 and 52 000) of human cardiac troponin in the Ca^{2+}-saturated form by X-ray crystallography. Analysis of the four structures derived from the two crystal forms reveals that the core domain is further divided into sub-domains, connected by linkers, making the entire molecule highly flexible. The structures of the troponin ternary complex suggests that the Ca^{2+}-binding to the regulatory TnC site displaces the carboxyl-terminal portion of TnI from actin/tropomyosin, thereby altering mobility and/or flexibility of the troponin/tropomyosin strand on the actin filament. These Ca^{2+}-dependent changes in the properties of the tropomyosin strand on the actin filament may in turn alter accessibility of myosin heads (motor protein) to the actin filament.

Keywords — troponin, muscle regulation, x-ray crystallography, calcium, EF-hand, synchrotron

Received — 18 February 2004, accepted 15 October 2004

Introduction

Muscle contraction is caused by interactions between two major contractile proteins, myosin and actin. In skeletal and cardiac muscle, either actin or myosin is polymerized to form filaments, the thin filament and the thick filament, respectively. The sliding action of these two filaments, which results in muscular contraction, is regulated by the intracellular Ca^{2+} concentrations. The molecular basis for Ca^{2+} regulation was initially established by Ebashi and co-workers in the 1960s, who identified troponin and tropomyosin as the principal proteins involved in this process [1]. Troponin, with a relative molecular mass of approximately 80 000 (80 kDa), is composed of three polypeptide chains, troponin T (TnT), troponin I (TnI) and troponin C (TnC) and is generally located along polymerized actin together with tropomyosin to form the backbone of the filament at a troponin : tropomyosin : actin ratio of 1 : 1 : 7 [2–5] (Fig. 1). Each subunit of the troponin complex performs a distinct function. TnT is the tropomyosin-binding subunit, TnI is the inhibitory subunit that blocks acto-myosin interactions and TnC is the Ca^{2+}-binding subunit that prevents TnI inhibition upon Ca^{2+} binding to its regulatory sites. The crystal structure of TnC reveals a dumbbell shaped structure with two globular domains connected by a central helix [6,7] (Fig. 2a). Each globular domain contains a pair of Ca^{2+}-binding sites. These sites in the N-terminal domain are specific for Ca^{2+} and responsible for regulation, while the C-terminal sites have a structural role and display higher affinity for Ca^{2+}. Moreover, the C-terminal sites are permanently occupied with Ca^{2+} or Mg^{2+} in the muscle cell. The crystal structure of TnC in complex with the N-terminal TnI peptide provides an insight into the mechanism of Ca^{2+} regulation [8]. The TnI fragment (residues 1–47) forms an amphiphilic α-helix that binds the hydrophobic cleft of the carboxyl-terminal domain of TnC (C-lobe) (Fig. 2b). Similar interaction in the amino-terminal domain (N-lobe) was proposed (Fig. 2c) on the

basis of this structure together with that of Ca^{2+}-saturated skeletal TnC in solution [9]. At a low Ca^{2+} concentration, the inhibitory region (IR, residues 137–148 in human cardiac TnI) interacts with actin, thereby blocking actomyosin ATPase activity [10–12]. Following an increase in Ca^{2+} concentration in the sarcoplasm, Ca^{2+} binding to the N-lobe facilitates accessibility of the hydrophobic patch for binding to the second amphiphilic α-helix of TnI, which is located immediately downstream of the inhibitory region. The inhibitory region detaches form actin/tropomyosin, resulting in the prevention of inhibition. Direct interactions between the N-lobe of TnC and the TnI amphiphilic segment have been confirmed by NMR [13]. Although there is little doubt that the alternation in the interactions between TnC and TnI reported here have a primary role in triggering the initiation of muscle contraction, the mechanism by which troponin regulates the interactions between myosin heads and the non-equivalent seven actin monomers remains elusive. Troponin is believed to be anchored in the thin filament mainly through TnT. Thus, elucidation of the ternary complex (TnT/TnI/TnC) structure is crucial to determine the molecular mechanism of Ca^{2+} regulation. Here we report the first crystal structures of the troponin ternary complex. Our data show that the three polypeptide chains are folded around each other within the troponin molecule, and provide an insight into the mechanism by which the signal of Ca^{2+} binding to the regulatory TnC site is transmitted to other thin filament proteins. Details of the crystallographic structure solution are discussed in a recent publication by our group [14]. In this manuscript, we review the main findings derived from the structures and discuss its possible contribution of Ca^{2+} to the regulatory mechanism of muscle contraction.

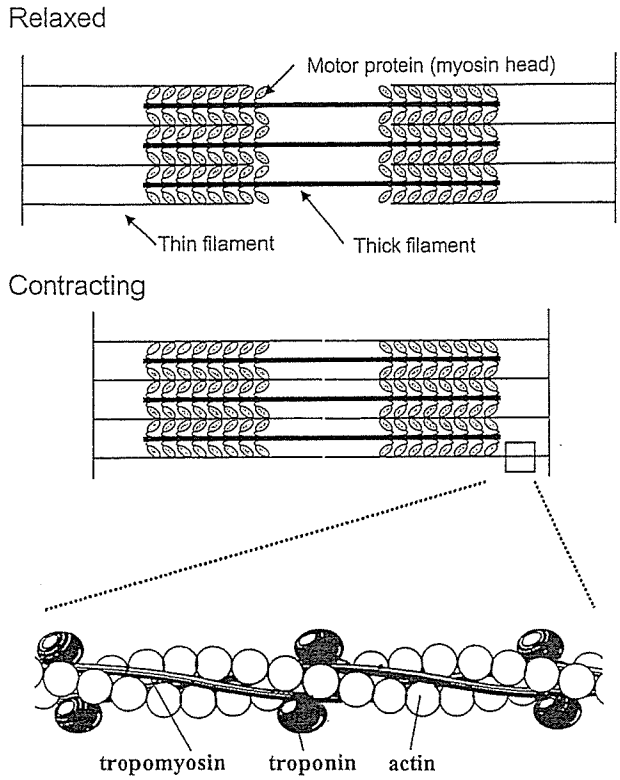

Fig. 1 Schematic representation of the ultrastructure of striated muscle.

Methods

Preparation

We crystallized two distinct preparations of the troponin core domain reconstituted from *Escherichia coli*-expressed recombinant human cardiac troponin subunits. One core domain consisting of TnC (residues, 1–161), TnI (residues, 31–163)

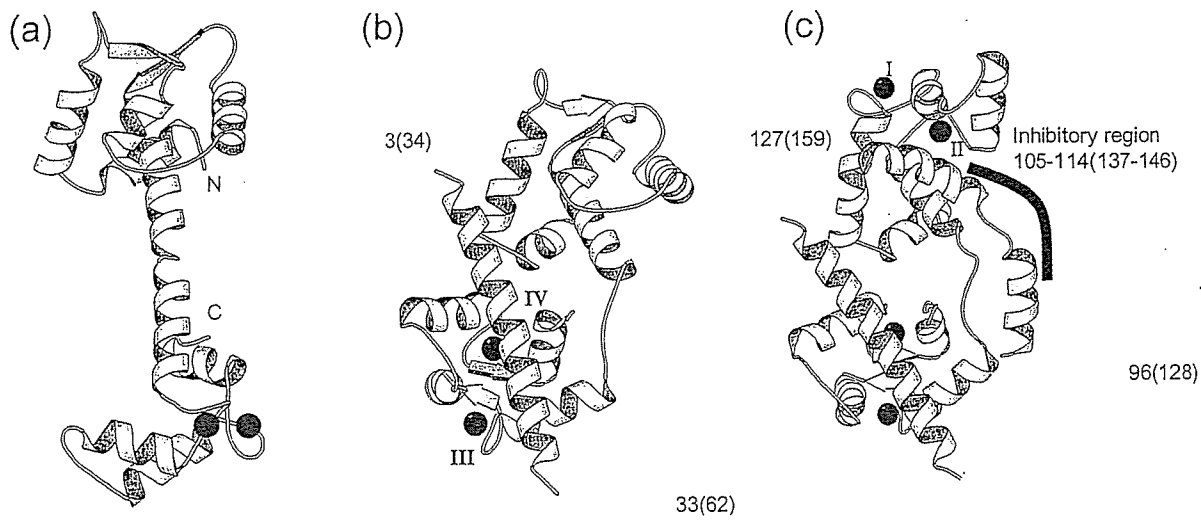

Fig. 2 Structures of TnCs. Crystal structure of TnC alone (a), TnC in complex with the N-terminal fragment of TnI (b), and a hypothetical model of TnC complexed with two putative TnC-binding segments of TnI (c). Amino acid numbers of the terminal residues of rabbit skeletal TnI segments and human cardiac TnI segments (in parentheses) are indicated. Bound Ca^{2+} ions (I–IV) are represented by black spheres.

and TnT (residues, 183–288) had a relative molecular mass of 46 K (Tn46K) and the other comprising TnC (1–161), TnI (31–210) and TnT (183–288) was 52 K (Tn52K). These core domains were equivalent to the chymotryptic fragments of rabbit skeletal Tn, which partially retain regulatory activity [15]. For TnI and TnC, cysteine-less variants (TnC (C35S/C84S) and TnI (C80A/C97)) were used to avoid the formation of the intermolecular disulfide bonds that prevent crystallization. Tn subunits were expressed and purified separately and dissolved in solution containing 6 M Urea. The mixture was dialyzed consecutively against NaCl solutions of 1, 0.5, 0.3 and 0.1 M, each containing 20 mM Tris/HCl at pH 8.0. Following refolding, the ternary complex was isolated by anion exchange chromatography and subjected to crystallization.

Crystallization

Native crystals were grown using the hanging-drop vapor diffusion technique with reservoir solution containing 20% polyethylene glycol (PEG) 3350, 15% glycerol, 0.1 M LiCl, 50 mM Tris/HCl and 5 mM $CaCl_2$, pH 8.0. Drops composed of 2 μl protein (10 mg ml^{-1}) and 2 μl reservoir solution were equilibrated with 0.5 ml reservoir solution for a minimum of two weeks at 20°C. Tn46K and Tn52K crystallized in space group $P2_1$ with unit cell dimensions of $a = 42.3$ Å, $b = 167.9$ Å, $c = 69.7$ Å, $\beta = 101.4°$, and $a = 48.3$ Å, $b = 169.5$ Å, $c = 68.5$ Å, $\beta = 102.4°$, respectively. Crystals were flash-frozen under nitrogen flow at 100 K after increasing the glycerol concentration 20% by soaking.

Structure determination

All diffraction data were collected at SPring-8 (the third generation synchrotron facility) in Japan (beam lines BL41XU, BL44B2 and BL45XU). Initial phases were obtained by the MAD (multiple anomalous dispersion) method [16] by using osmium and strontium derivatives of Tn46K crystals. The model was refined against the native Tn46K dataset to 2.6 Å resolution with a crystallographic R-factor of 26.4% (R-free = 29.8%). The Tn52K structure was solved by the molecular replacement method using the refined Tn46K model and refined to 3.3 Å resolution with a crystallographic R-factor of 25.1% (R-free = 30.8%). The asymmetric unit of each crystal form contained two troponin molecules. We resolved the structures of four molecules in total, designated Tn46KA, Tn46KB, Tn52KA and Tn52KB. Atomic coordinates and structure factors have been deposited in the Protein Data Bank under the accession codes 1J1D for Tn46K and 1D1E for Tn52K.

Results and discussion

Structure description

The overall architecture of the Tn52KB is depicted in Fig. 3a. Notably, the core domain of troponin is dominated by α-helices. To date, structures have been solved in the presence of Ca^{2+}. Thus, all three functional Ca^{2+}-binding sites (II, III and IV) are occupied (site I is not functional in cardiac TnC). The core domain is further subdivided into structurally distinct sub-domains, denoted the regulatory head and the IT-arm. The IT-arm has an asymmetric and elongated structure (~80 Å), which is mainly stabilized through two characteristic sets of interactions between the subunits. One comprises a parallel α-helical coiled-coil formed between the carboxyl-terminal portion of TnT (H2(T2)) and the middle portion of TnI (H2(I)). Each chain has 6.5 heptad repeats with hydrophobic residues at *a* and *d* positions, which are highly conserved among species [17]. The other involves hydrophobic interactions formed between the amino-terminal amphiphilic α-helix H1(I) of TnI and the hydrophobic cleft of the carboxyl-terminal domain (C-lobe) of TnC. As specified in Section 2, the metal binding sites in the C-lobe are permanently occupied by metal ions, irrespective of sarcoplasmic Ca^{2+} concentrations. Here, helix H2(T2) interacts with TnI by forming a coiled-coil on one side. The other side of the helix directly interacts with the Ca^{2+} binding loops of TnC C-lobe. Since the C-lobe is rigidly integrated into the IT-arm, this structure may remain unchanged irrespective of the physiological state of the thin filament. On the other hand, the regulatory head consists of the amino-terminal lobe of TnC (N-lobe) and the bound amphiphilic α-helix of TnI (H3(I)). As suggested previously [8,13], the amphiphilic H3(I) α-helix binds specifically to a conserved hydrophobic patch of the Ca^{2+}-saturated N-lobe of TnC in a Ca^{2+}-dependent manner. The H3(I) segment is located between the two putative actin/tropomyosin-binding sites, the inhibitory region and the carboxyl-terminus of TnI (C-TnI), which are both essential for inhibitory binding of TnI at a low sarcoplasmic Ca^{2+} concentration [12,18]. The structure of each sub-domain is almost identical in all four molecules, indicating that each sub-domain behaves as an individual unit. However the relative orientation between the two sub-domains is fairly variable (Fig. 3b). The largest differences are observed between Tn46KA and Tn46KB, where the IT-arm is rotated by 20° relative to the regulatory head, leading to a 27 Å displacement at the distal end of the IT-arm. Direct contacts between the IT-arm and the regulatory head are mediated by a small number of amino acid residues that are poorly conserved among the species. Therefore, the contacts are eventually stabilized by crystal-packing. Moreover, covalent links between the sub-domains involving the linkers connecting the D- and E-helices of TnC and the inhibitory region of TnI (between H2(I) and H3(I)) are not well defined in electron density maps suggesting that these linkers work as a universal joint. These findings collectively suggest that troponin molecule adopts multiple conformations with variable sub-domain orientations both on the muscle filament and within the crystal. Since troponin is fairly flexible, the molecule evades packing in the crystalline lattice for a long time.

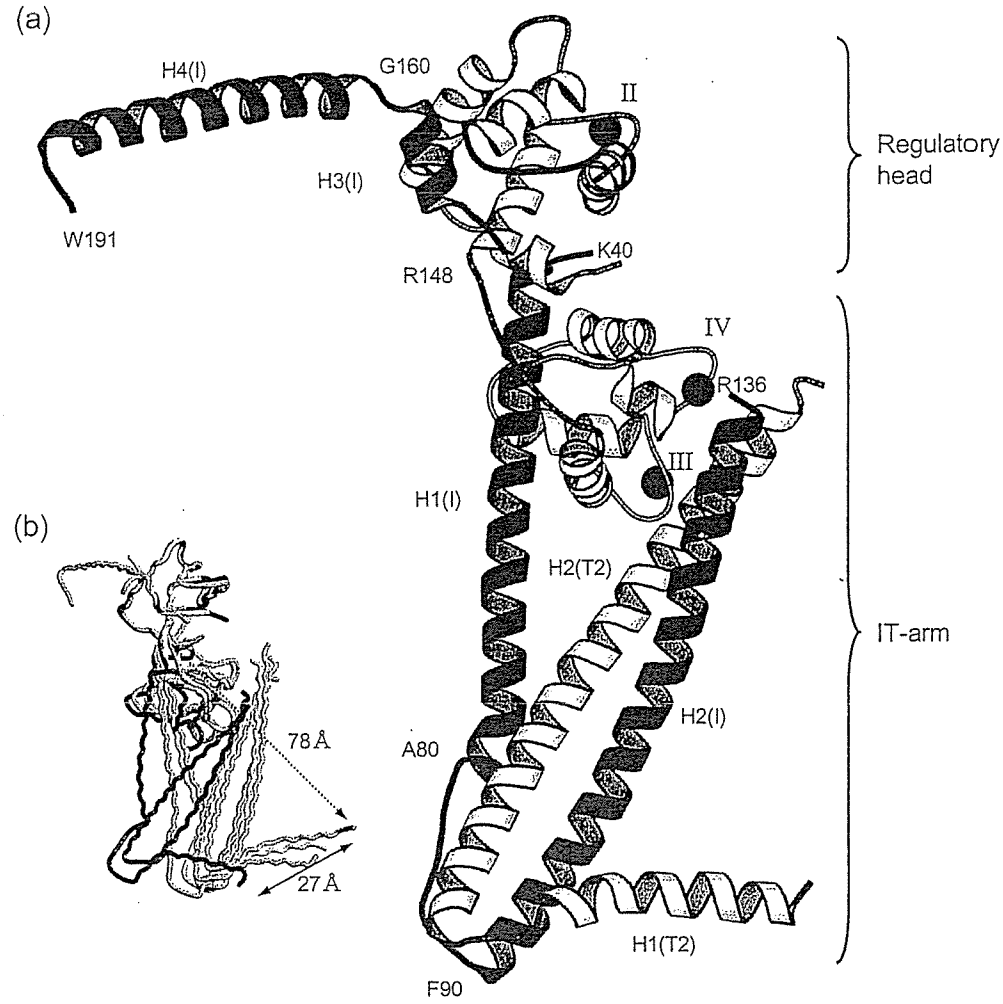

Fig. 3 Crystal structures of the core domain of human cardiac troponin. Ribbon representation of the Tn52KB molecule structure (a), and the superimposition of the four molecule structures with the best superimposition (least-square fit) of the regulatory head (b). The three bound Ca^{2+} ions (II–IV) are represented by black spheres.

Interactions between troponin and other thin filament components

Troponin is anchored to the thin filament mainly through tropomyosin binding to two distinct portions of TnT, specifically the amino-terminus (TnT1, residues 1–182) and the carboxyl-terminus (C-TnT, residues 272–288), irrespective of the sarcoplasmic Ca^{2+} concentrations (Fig. 4). The three-dimensional structure of TnT1 is currently unknown. However, a number of reports show that TnT1 has high α-helical content and is less susceptible to proteolysis, indicating that it forms a separate structural domain. On the basis of the present structures, the separation between TnT1 and C-TnT is estimated as 60 Å, although these two structural subdomains are not included in the current crystal structure. No part of the IT-arm has direct interactions with actin or tropomyosin. At low Ca^{2+} concentrations, the N-lobe of TnC dissociates from the H3(I) helix, resulting in another attachment of the carboxyl-terminal portion of TnI, denotes 'regulatory segment of TnI' (TnI_{reg}, residues 137–210) to the filament possibly to generate the ternary complex of actin/tropomyosin/TnI_{reg} [15].

Molecular mechanism of muscle regulation

During Ca^{2+} regulation, TnI_{reg} undergoes major changes, both with regard to position and conformation. At the high Ca^{2+} concentrations, TnI_{reg} associated with the N-lobe of TnC detaches from actin/tropomyosin as observed from the present crystal structure. On the other hand, at low Ca^{2+} concentrations, TnI_{reg} must form an extra attachment to actin/tropomyosin so that the troponin/tropomyosin strand is tied down to the actin filament (Fig. 4). The IT-arm may have an important role in the regulatory process. This subdomain is large, rigid and conserved between species and has no direct interactions with actin/tropomyosin. Moreover the location is interesting. The structure bridges two Ca^{2+}-independent attachments to actin/tropomyosin, specifically, TnT1 and C-TnT. The IT-arm resides immediately downstream of the tropomyosin anchoring site (C-TnT) and mobile TnI_{reg}. An intriguing possibility is that the formation of a third attachment by TnI_{reg} at low Ca^{2+} concentrations causes a minute rotation of the IT-arm about the pivotal point—the C-terminal end of the coiled-coil. The formation of the third attachment itself, as well as the rotation of the

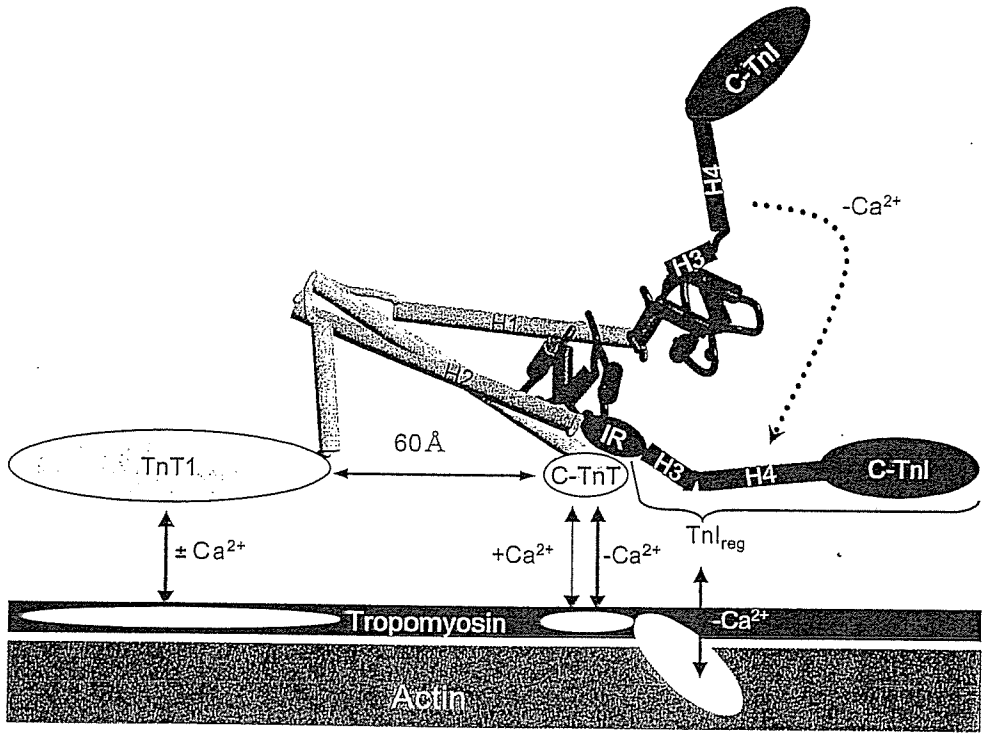

Fig. 4 Schematic representation of the interactions between troponin and other thin filament components. Potential actin/tropomyosin-binding portions, which are not included in the current structural model (TnT1, C-TnT, C-TnI and IR) are shown.

IT-arm, may alter the properties of the tropomyosin strand on the actin filament.

It is almost 30 years since the idea was put forward that tropomyosin acts, at least in part, by changing positions on actin, thus uncovering or modifying the myosin-binding site on actin when troponin binds Ca^{2+} (Fig. 5a). Although previous results are consistent with this steric blocking mechanism [19–21], the systematic fluorescence resonance energy transfer (FRET) experiment consistently failed to provide evidence of any major changes in the distance between tropomyosin and actin [22]. A more plausible explanation is that the strain imposed on the tropomyosin strand is altered. Consequently the mobility and/or flexibility of the tropomyosin strand is changed, which in turn modifies the accessibility of the myosin head to binding sites on the actin filament (Fig. 5b). Alternatively, it is possible that enhanced flexibility of the tropomyosin strand leads to conformational changes in actin subunits that induce higher flexural rigidity of the actin filament. The thin filament is more flexible in the presence of Ca^{2+} and its bending motion is accelerated by interactions of myosin heads with Mg^{2+}-ATP [23,24].

The nature of the changes in the thin filament remains to be elucidated. To determine the molecular mechanism of muscle regulation, it is crucial to clarify high-resolution structures of the whole thin filament complex (actin/tropomyosin/troponin) corresponding to each state during the contractile cycle [25]. Notably, thin filament-associated X-ray diffraction intensities [19–21] as well as electron micrographs [26] have been interpreted based on the assumption that the mass of the troponin/tropomyosin complex is distributed evenly and smoothly throughout the continuous 'tropomyosin strand'. With the present atomic structures, trials are currently underway to separately identify the mass of tropomyosin and that of troponin on the muscle thin filament.

Concluding remarks

The present study reveals that troponin can be divided into sub-domains, specifically, the regulatory head, the IT-arm, TnT1, C-TnT and TnI_{reg}. These sub-domains are connected by linkers, making the entire molecule fairly flexible. The crystal structures additionally provide an opportunity to visualize sites of genetic disorder in the troponin molecule that are associated with cardiac dysfunction [27]. In conjunction with previous results, data from the present structures enable us to outline a working hypothesis. Specifically, Ca^{2+} binding to the N-lobe of TnC induces interactions to the switch (H3(I) helix in TnI_{reg}) leading to the detachment of the entire TnI_{reg} from actin/tropomysin. This removal of TnI_{reg} releases the strain imposed on the tropomyosin strand via readjustment of the posture of the IT-arm. Changes in the properties of the tropomyosin strand may modify the accessibility of the myosin head to actin. Although this is the first hypothesis to explain the mechanism by which troponin works on the basis of its atomic structures, further work is necessary to establish complete understanding of the